筑波大学

博士（医学）学位論文

Role and regulation of transcription factor Myb in cell cycle progression.

（細胞周期の進行における転写因子 Myb の役割とその調節）

2007

筑波大学大学院人間総合科学研究科

山内　智弘

目次

序章

myb はもともと、ニワトリ骨髄性白血病ウイルスが持つがん遺伝子（v-*myb*）として同定され、c-*myb* 遺伝子が、その細胞側ホモログとして同定された。c-*myb* 遺伝子産物（c-Myb）は、N 末端側に 51～53 アミノ酸を単位とする３つのリピート構造から成る DNA 結合ドメインを有し、このドメインを介して、DNA 配列 5'-AACNG-3'に結合する。そして DNA 結合ドメインの C 端側には、酸性アミノ産に富む転写活性化ドメインが存在し、この領域に転写コアクティベーターCBP が結合し、c-Myb による転写活性化を仲介することが知られている。

動物において、c-Myb と構造が類似する因子として、A-Myb と B-Myb の２つが同定され、これらの３つの Myb ファミリー転写因子の構造と機能が、これまでに研究されてきた。A-Myb, B-Myb, c-Myb はいずれも良く保存された DNA 結合ドメインを有し、同一 DNA 配列 5'-AACNG-3'に結合する。また、これらの Myb ファミリー転写因子は、その程度に差はあるものの、いずれも転写を活性化する能力を有している。しかし、これらの３つの因子は、その発現パターンに大きな違いがある。c-*myb* は未成熟造血系細胞で発現が高く、分化の進行に伴いその発現は低下する。c-*myb* ノックアウトマウスは、胎児肝臓での造血不全や、胸腺での T 細胞の分化異常を呈する。このことから、c-Myb は、未分化造血細胞の増殖や T 細胞の初期発生に必須であると考えられる。一方、A-*myb* は精巣や乳腺で発現が高く、A-*myb* ノックアウトマウスは、精子形成異常や妊娠時の乳腺形成異常を呈する。従って、A-Myb はこれらの生殖機能特異的な組織における未分化細胞の増殖や分化に重要な役割を果たしていると考えられる。これら２つの Myb ファミリー転写因子と異なり、B-*myb* は、ほぼ全てのタイプの細胞に発現しており、B-*myb* 欠損マウスは発生早期に致死となる。このことから、B-*myb* は多くの細胞における細胞増殖の制御などにおいて、普遍的な役割を担っていると推察されるが、その実態は不明な点が多い。

Myb ファミリー転写因子の生理機能を明らかにするために、これまで幾つかの Myb に結合する因子が同定され、解析されてきた。特に、最近５年間に B-Myb 複合体とショウジョウバエ Myb 複合体の解析は、大きく進展した。ショウジョウバエは *myb* 遺伝子を一つだけ有しており、その変異体は細胞周期の進行やゲノム安定性の異常が見られる。動物細胞の３つの myb 遺伝子をショウジョウバエ *myb*（*dmyb*）変異体に戻す実験から、３つの動物 Myb ファミリー転写因子のうち、B-Myb が最も dMyb に機能的に近いことが示されている。そして実際にゼブラフィッシュの B-*myb* 変異体も、*dmyb* 変異体と同様に、ゲノム不安定性を示すことが報告されている。EMBL と米国の２つのグループによって、dMyb を含む複合体が精製され、この複合体は、ショウジョウバエの E2F や Rb などの一群の因子を含むことが示された。この複合体は、最初 dREAM 複合体（dRBF、dE2F2、and dMyb-interacting proteins）と名付けられた。

一方、この複合体に含まれる因子が、C. elegans の陰門形成異常を指標として同定された一群の遺伝子（synthetic multivulva class B genes）の産物に相当することから、これは Myb-MuvB 複合体とも呼ばれている。最近では、このような dMyb 複合体の形成と同様に、動物細胞の B-Myb も Rb や E2F などの因子と dREAM/Myb-MuvB-like 複合体を形成することが示されている。そして、この複合体は、*cyclin* B1 のような G2/M 期の進行に必須の遺伝子群の転写を活性化することが明らかにされている。しかし、*dmyb* や B-*myb* 変異体における、ゲノム不安定性が、G2/M 移行の異常だけによって、完全に説明できるか否か、などの幾つかの重要な疑問が残っている。

一方 c-Myb については、これまでに、CBP などの転写コアクティベーター、Ski や TIF1b などのコリプレッサー、そして、NLK や HIPK2 などのキナーゼが、直接 c-Myb に結合することが示された。これらのコアクティーベーターとコリプレッサーは競合的に c-Myb に結合し、c-Myb 活性を、それぞれ正と負に制御することが示されている。また NLK と HIPK2 の解析から、Wnt シグナルが TAK1→HIPK2→NLK 経路を介して、NLK を活性化し、NLK が直接 c-Myb をリン酸化し、プロテアソーム依存的な c-Myb タンパク質の分解を誘導することも報告されている。Myb-binding protein 1a （Mybbp1a）は、もともと c-Myb のロイシン rich 領域を含むドメインに結合する因子として同定された因子である。この因子は、160kD の Mybbp1a（$p160^{MBP}$）と、それがプロセッシングされて生じる N 末側 67kD のフラグメント（$p67^{MBP}$）の２つの存在状態を取る。$p160^{MBP}$ と $p67^{MBP}$ は共に c-Myb に結合するが、興味深いことに、$p67^{MBP}$ のみが c-Myb の転写活性化能を抑制できる。さらに Mybbp1a の一部は核質にも局在するが、大部分は核小体に局在している。そして、$p160^{MBP}$ の核・核小体局在のためには、C 末側にある複数の Basic アミノ酸リピート配列が重要であることが分かっている。しかし、$p160^{MBP}$ のプロセッシングや $p160^{MBP}$ による Myb 活性制御の生理的役割については、不明な点が多い。

私は、Myb に結合する因子を精製・解析し、それによって Myb ファミリー転写因子の生理機能を明らかにすることを試みた。まず、B-Myb を含む複合体の精製を試み、これまでに報告されていない新たな B-Myb 複合体を精製した。また、c-Myb に結合する Mybbp1a の複合体の精製を試み、Mybbp1a の生理機能の解明を試みた。

第一章

A B-Myb Complex Containing Clathrin and Filamin Is Required for Mitotic Spindle Function

Tomohiro Yamauchi,[1,2]* Takefumi Ishidao,[1]* Yasunori Tanaka,[1] Toshie Shinagawa,[1] Shigenobu Yonemura,[3] and Shunsuke Ishii[1,2]**

[1]Laboratory of Molecular Genetics, RIKEN Tsukuba Institute, 3-1-1 Koyadai, Tsukuba, Ibaraki 305-0074, Japan
[2]University of Tsukuba, Graduate School of Comprehensive Human Sciences, 1-1-1 Tennoudai, Tsukuba, Ibaraki 305-8577, Japan
[3]Laboratory for Cellular Morphogenesis, RIKEN Center for Developmental Biology, 2-2-3 Minatojima-minamimachi, Chuo-ku, Kobe 650-0047, Japan

*These authors contributed equally to this work.

**Correspondence: E-mail: sishii@rtc.riken.jp

Running title: B-Myb Regulates Mitotic Spindle Function

SUMMARY

B-Myb is one member of the vertebrate Myb family of transcription factors and is ubiquitously expressed. B-Myb activates transcription of a group of genes required for the G2/M cell cycle transition by forming the dREAM/Myb-MuvB-like complex, which was originally identified in *Drosophila*. Mutants of zebrafish B-*myb* and *Drosophila myb* exhibit defects in cell cycle progression and genome instability. Although the genome instability observed in the B-*myb* mutant has been speculated to be due to abnormal cell cycle progression, the precise mechanism remains unknown. Here, we have purified a B-Myb complex containing clathrin and filamin (Myb-Clafi complex), which is concentrated at the mitotic spindle. This complex is required for normal localization of clathrin at the mitotic spindle, which was previously reported to stabilize kinetochore fibres. Thus, identification of the Myb-Clafi complex reveals a previously unrecognized function of B-Myb that may contribute to its role in chromosome stability, possibly, tumor suppression.

INTRODUCTION

The Myb family of transcription factors play important roles in proliferation and differentiation (Oh and Reddy, 1999). The vertebrate *myb* gene family contains three members, A-*myb* and B-*myb*, in addition to c-*myb*, the cellular progenitor of the v-*myb* oncogene (Nomura et al., 1988). The level of c-*myb* expression is high in immature hematopoietic cells (Gonda and Metcalf, 1984), and analysis of c-*myb* KO mice revealed that c-*myb* is required for definitive hematopoiesis and T cell development at several stages (Mucenski et al., 1991; Bender et al., 2004). A-*myb* is also highly expressed in the limited types of cells such as testis and breast (Trauth et al., 1994), and is required for spermatogenesis and development of breast tissue following pregnancy (Toscani et al., 1997). In contrast to c-*myb* and A-*myb*, B-*myb* is ubiquitously expressed (Nomura et al., 1988) and the B-*myb* mutant mice die early in development (Tanaka et al., 1999), suggesting the universal role of B-*myb* gene product (B-Myb) in many types of cells.

All the three members of vertebrate Myb family proteins have the conserved DNA-binding domain (DBD), which recognizes the specific DNA sequence 5'-AACNG-3' (Ogata et al., 1994). The transcriptional activation domain containing the acidic amino acid-rich region is also localized adjacent to the DBD in all the three members (Sakura et al., 1989; Nakagoshi et al., 1993), which bind to the transcriptional coactivator CBP (Dai et al., 1996; Bessa et al., 2001). B-Myb is induced at G1/S in the cell cycle and is activated by cyclinA-cdk2-dependent phosphorylation (Robinson et al., 1996), suggesting an important role in cell cycle control.

Of the vertebrate Myb proteins, B-Myb is most closely related to *Drosophila* Myb (dMyb) (Davidson et al., 2005). Mutants of d*myb* and zebrafish B-*myb* exhibit defects in cell cycle progression (Katzen et al., 1998; Okada et al., 2002) and genome instability (Fung et al., 2002; Manak et al., 2002; Manak et al., 2007; Shepard et al., 2005). dMyb forms a multisubunit protein complex that is essential for silencing of developmentally regulated genes (Korenjak et al., 2004; Lewis et al., 2004). This complex, referred to as dREAM/Myb-MuvB complex, contained dMyb, RBF, E2F, DP, in addition to the previously identified dMyb-interacting proteins Mip120, Mip130, and Mip40 (Beall et al., 2002; Beall et al., 2004). Interestingly, *C. elegans* homologs for each component of this are products of the synthetic multivulva class B (synMuvB) genes that function to antagonize Ras signaling in development of the vulva (Ceol et al., 2006; Fay and Han, 2000). The *C. elegans* synMuvB gene products form a complex termed Dpl-Rb-MuvB (DRM) similar in composition to the dREAM/Myb-MuvB complex (Harrison et al., 2006). Similar to dMyb, B-Myb forms the dREAM/Myb-MuvB-like complex containing p130, a member of RB family, E2F4, and LIN-9, a homolog of Mip130, and activates transcription of a group of genes such as cyclin B1, which are required for the G2/M cell cycle transition (Zhu et al., 2004;

Osterloh et al., 2006; Pilkinton et al., 2007; Litovchick et al., 2007).

The genome instability caused by the mutations of d*myb* and B-*myb* is speculated to be due to abnormal cell cycle progression, especially at the G2/M transition, but the precise mechanism remains unknown. Here, we have purified a B-Myb complex containing clathrin and filamin, which is concentrated at the mitotic spindle. Disruption of this complex has led to genome instability, suggesting that B-Myb directly functions for the mitotic spindle.

RESULTS

Purification of Myb-Clafi Complex which Is Abundant in the M-phase Cells

The HeLa S3 cell line, in which FLAG/HA-B-Myb is stably expressed, was generated by retroviral transduction. Western blotting analysis indicated that two clones (clone 7 and 9) among several isolated lines expressed FLAG/HA-B-Myb at levels similar to that of endogenous B-Myb (Fig. 1A). Clone 7 was cultured to purify the B-Myb complex. Cells were disrupted in hypotonic buffer, and the pellets which mainly contained the nuclei were isolated. The B-Myb complex was purified from the extracts of the pellets by sequential immunoprecipitation with anti-FLAG and anti-HA antibodies, as described by Nakatani and Ogryzko (2003). Silver staining of SDS-PAGE gels of the purified proteins indicated that, in addition to FLAG/HA-B-Myb, the complex contained two high molecular weight bands of 280- and 160-kD, which were not detected in the purified sample from control HeLa cells not expressing epitope-tagged proteins (Fig. 1B). Analysis of the FLAG-purified B-Myb complex using glycerol gradient centrifugation indicated that only these two large proteins were detected in the B-Myb containing fractions (Fig. 2A). Mass spectrometric analysis indicated that the 280-kD band contained filamin A and α-spectrin, while the 160-kD band was the clathrin heavy chain (CHC). Western blotting using specific antibodies indicated that filamin A was detected in the B-Myb concentrating fractions, whereas α-spectrin was concentrated in the slightly higher molecular weight fraction (Fig. 2B). Thus, the B-Myb complex containing clathrin and filamin A was concentrated in fractions 11 and 12, while a- and b-spectrin, which may form a heterodimer, were concentrated in the fractions 13 and 14. We designated this complex Myb-Clafi for the Myb complex containing clathrin and filamin. The molecular weight of the Myb-Clafi complex is approximately 500-600 kD, suggesting that this complex consists of one molecule each of filamin A, CHC, CLC, and B-Myb.

To examine the abundance of the Myb-Clafi complex during cell cycle, we prepared synchronized HeLa cells. HeLa cells expressing FLAG/HA-B-Myb were synchronized at the G1-S boundary by the double thymidine-block protocol, and the cell cycle distribution in G1, S, or G2/M was determined by fluorescence activated cell sorting (FACS) analysis of cells at various times after release of the block (Fig. 3). The results indicated that a substantial fraction of the cells was synchronized by this protocol. To examine the abundance of B-Myb itself throughout the cell cycle, lysates were prepared at various times after release of the thymidine block. The level of B-Myb was highest in S phase and early G2/M phase (Fig. 4A). At M-phase, the B-Myb level decreased, but continued to be present at low levels through the G1 phase.

Under the same salt concentration as the Myb-Clafi complex purification, CHC, CLC, and filamin A co-precipitated with FLAG/HA-B-Myb only in cytosolic lysates of G2/M phase-enriched cells, but not in the nuclear fraction (Fig. 4B). When nuclear fractions from different stages of the cell cycle were used, small amounts of CHC co-precipitated with FLAG/HA-B-Myb, but neither filamin A nor CLC were present (Fig. 4B). These results suggest that CHC may regulate B-Myb-dependent transcription. A similar association between CHC and p53 was recently reported (Enari et al., 2006). To examine whether endogenous B-Myb forms the Myb-Clafi complex, we performed co-immunoprecipittaion using HeLa cells. Anti-B-Myb antibody co-precipitated endogenous clathrin and filamin from cytosolic extracts of G2/M-phase-enriched cells, while control IgG did not (Fig. 4C). When we used lysates of unsynchronized cells, we could not observe this type of specific co-immunoprecipitation. Thus, the Myb-Clafi complex is abundant in the cytosolic fraction of M-phase cells. The complex was originally purified from the extracts of nuclear pellets, but this localization may have been the result of an incomplete separation of nuclear and cytosolic fractions of M-phase cells.

Localization of B-Myb at the Mitotic Spindles

Clathrin functions in the generation of vesicles that transfer membrane and proteins between intracellular compartments (Edeling et al., 2006). Independent of this function, clathrin was reported to be localized on and required for the function of the mitotic spindle (Okamoto et al., 2000; Royle et al., 2005). Filamin is an actin crosslinking and molecular scaffold protein (Popowicz et al., 2006; Feng and Walsh, 2004). These results raised the possibility that the Myb-Clafi complex is localized at the mitotic spindle. To examine the localization of endogenous B-Myb, synchronized HeLa cells were immunostained with anti-B-Myb. At interphase, B-Myb was observed in the nucleus in dot-like structures (Fig. 5A). In M-phase cells, B-Myb was detected at the kinetochore fibres after washing out cytosolic proteins with Triton X-100 treatment prior to fixation, which is commonly used to detect microtubule-associated proteins (Fig. 5A). Since the endogenous B-Myb signals were weak, we generated a HeLa cell line expressing a fusion of Venus, a GFP derivative (Nagai et al., 2002), with B-Myb (Venus-B-Myb). HeLa cells were infected with a retrovirus vector encoding Venus-B-Myb and then isolated. In

cells expressing Venus-B-Myb, Venus-B-Myb was clearly detected at the kinetochore fibres of M-phase cells, while it was observed in the nucleus of interphase cells with some dot-like structures as seen in the case of endogenous B-Myb (Fig. 5B).

Localization of the B-Myb/E2Fs Complex on Condensed Chromosomes

When HeLa cells were treated with 1% Triton X-100 for 10 min, endogenous B-Myb and Venus-B-Myb were detected only at the kinetochore fibres in metaphase cells (Fig. 5). However, when weaker detergent extraction conditions (1% Triton X-100 for 1 min) were used prior to fixation, a strong Venus-B-Myb signal was also detected on condensed chromosomes at various stages in M-phase (Fig. 6A). E2F1/4 were similarly observed on condensed chromosomes in metaphase cells after treatment with 1% Triton X-100 for 5 min (Fig. 6B). B-Myb binds to E2Fs (Zhu et al., 2004; Osterloh et al., 2006, Pilkinton et al., 2007; Litovchick et al., 2007), similar to dMyb in the dREAM/Myb-MuvB complex (Korenjak et al., 2004; Lewis et al., 2004). Therefore, these results suggest that B-Myb on the condensed chromosomes corresponds to the-B-Myb/E2Fs complex, not the Myb-Clafi complex. The B-Myb signals detected on the condensed chromosmomes may be washed out when the strong detergent condition (1% Triton X-100 for 10 min) was used prior to fixation. On the other hand, the B-Myb signals on the mitotic spindles were hard to detect when the weak (1% Triton X-100 for 1 or 5 min or no detergent) or no detergent washing was used, because they are very weak compared to the signals on the condensed chromosomes. These results are consistent with the fact that the Myb-Clafi complex, which was purified using 0.42 M salt concentration, may be more stable and much less abundant than the dREAM/Myb-MuvB-like complex, which was purified using 0.1 M salt concentration (Korenjak et al., 2004; Lewis et al., 2004).

Decrease in B-Myb Reduces Clathrin on the Mitotic Spindles and Leads to Mitotic Arrest

To investigate the importance of B-Myb in the localization of clathrin at the kinetochore fibres, we combined cell synchronization with RNAi. HeLa cells were transfected with a small interfering RNA (siRNA) during the interval between the two thymidine blocks and were examined for expression of B-Myb 6-9 h after release into the cell cycle. Transfection of cells with siRNAs specific for B-Myb resulted in a specific reduction in the level of B-Myb (Fig. 7A). Depletion of B-Myb did not affect the levels of clathrin and filamin (Fig. 7A), but markedly impaired the localization of endogenous CHC (Fig. 8A) and exogenously expressed EGFP-CLC to the kinetochore fibres (Fig. 8B). These results are consistent with the B-Myb-Clafi complex being localized to the mitotic spindle.

Depletion of B-Myb markedly impaired the ability of HeLa cells to progress through mitosis, whereas transfection of cells with a control siRNA had no such effect. The B-Myb-depleted cells took an unusually long time to complete mitosis, displayed marked difficulties in completing cytokinesis, and finally had an apoptosis-like phenomena (Fig. 7B). The proportion of cells in mitosis increased 4.9 fold in the B-Myb-depleted cells compared to the control siRNA-treated cells (Fig. 8C). In B-Myb-depleted cells, the metaphase plate was thicker than in the control cells and there was an increased incidence of misaligned chromosomes (Fig. 8D, E). These severe effects of B-*myb* siRNA on mitosis might be the result of two different mechanisms: disruption of the Myb-Clafi complex and decreased expression of B-Myb target genes mediated by the dREAM/Myb-MuvB-like complex, which were recently shown to be required for G2/M transition (Zhu et al., 2004; Pilkinton et al., 2006; Osterloh et al., 2006; Litovchick et al., 2007).

M14 Mutant Can Form the dREAM/Myb-MuvB-like complex, but not the Myb-Clafi Complex

To examine the specific role of the Myb-Clafi complex during mitosis, especially by separating it from that of the dREAM/Myb-MuvB-like complex, we have used the B-Myb mutant 14 (M14). The M14 mutant cannot form the Myb-Clafi complex, but still retain the *trans*-activating capacity mediated by the dREAM/Myb-MuvB-like complex. M14 lacks the 118-amino acid region (aa 509-628) in the C-proximal region of B-Myb (Fig. 9A). Previously we demonstrated that M14 can stimulate transcription from the Myb site-containing promoter in a transient transfection assays (Nakagoshi et al., 1993). In co-immunoprecipitations using lysates from HeLa cells transfected with the M14 or wild-type (WT) B-Myb expression vector, clathrin and filamin A co-precipitated with WT B-Myb, but not with M14 (Fig. 9B). Human LIN-9 (hLIN-9), which is a component of the human dREAM/Myb-MuvB-like complex (Litovchick et al., 2007), co-precipitated with both WT and M14 B-Myb (Fig. 9C), suggesting that M14 retains the *trans*-activating capacity.

To generate cells expressing the M14 B-Myb mutant instead of endogenous wild-type (WT) B-Myb, we first produced B-*myb* conditional knockout mice using homologous recombination in ES cells. A targeting vector was constructed in which loxP sites were introduced 5' of exon 5, which encodes amino acids 94-167, corresponding to the essential region of the DNA-binding domain (Fig. 10A). A neomycin resistance (neo) cassette driven by the phosphoglycerate kinase (PGK) gene promoter and flanked by loxP sites was inserted in the intron located 3' to exon 5. To increase the frequency of gene targeting, the diphtheria toxin-poly(A) signal cassette for negative selection was fused to the short arm as described (Yagi et al., 1993). Homologous recombinants (fNeo allele) were characterized by the appearance of a 10.0 kb *Eco*RV fragment with the 5'-probe and an 8.6 kb *Nco*I fragment with the 3'-probe (Figs. 10A, B). In addition, the presence of three loxP sites was confirmed by DNA sequencing using the appropriate primers. To remove the neo cassette, ES cells harboring the fNeo allele were

transfected with the Cre recombinase expression vector. The f allele generated by deletion of the neo cassette was confirmed by the appearance of an 11.3 kb *Eco*RV fragment with the 5'-probe (Figs. 10A, B). Furthermore, the presence of two loxP sites was confirmed by DNA sequencing using the appropriate primers, and also by polymerase chain reaction (PCR) analysis using two primers, BMlox1 and Blox2. The f allele generates a 213-bp fragment, whereas the wild-type allele produces a 125-bp fragment (Figs. 10A, C). Chimeras were obtained from three independent mutant ES clones harboring the f/+ alleles and mated with C57BL/6 females to generate F1 heterozygous mutant mice. Intercrosses between heterozygotes yielded the homozygous mutants (f/f). Mouse embryonic fibroblasts (MEFs) were prepared from E14.5 embryos from wild type (+/+), heterozygous (f/+), and homozygous (f/f) mice. When MEFs were infected with lentivirus encoding the Cre recombinase, a deletion of the loxP-flanked sequences occurred, which were detected by PCR using the BMlox2 and BMlox3 primers. The deleted allele generates a 310-bp fragment, while the wild-type and f alleles each produce a 3200 bp fragment (Figs. 10A, D).

When the Cre recombinase was expressed in B-*myb*$^{f/f}$ mouse embryonic fibroblasts (MEFs), endogenous B-Myb was almost completely undetectable (Fig. 9D). To exogenously express M14 or WT B-Myb as a control, B-*myb*$^{f/f}$ MEFs were first infected with the Cre lentivirus, and then re-infected with adenoviruses encoding either M14 or WT B-Myb, which produced levels of B-Myb similar to wild-type MEFs (Fig. 9D). In B-Myb-depleted MEFs, the mRNA levels of seven G2/M genes, which are regulated by B-Myb and hLin-9 (Zhu et al., 2004; Osterloh et al., 2006), were lower than those of control cells (Fig. 9E). However, re-expression of either WT or M14 B-Myb efficiently rescued the decrease in these mRNA levels. Thus, M14 can activate the transcription of a cluster of B-Myb target genes. In M14-reexpressing cells (f/f:Cre+M14) and B-Myb-deficient cells (f/f:Cre), the CHC signals at kinetochore fibres were dramatically reduced, while CHC was prominently localized to the mitotic spindle in WT B-Myb-reexpressing cells (f/f:Cre+WT)(Fig. 9F). Thus, the ability of B-Myb to form the Myb-Clafi complex is correlated with that of B-Myb to localize clathrin to the kinetochore fibres.

Defects in Mitosis of MEFs Expressing M14 Instead of Endogenous WT B-Myb

To investigate the role of the B-Myb-Clafi complex during mitosis, we examined mitotic progression in four types of MEFs: control wild-type MEFs (+/+), B-Myb-deficient cells which were generated by infecting B-*myb*$^{f/f}$ MEFs cells with the Cre lentivirus (f/f:Cre), cells expressing M14 instead of endogenous B-Myb which were generated by sequentially infecting B-*myb*$^{f/f}$ MEFs cells with the Cre lentivirus and the M14-encoding adenovirus (f/f:Cre+M14), and B-Myb-reexpressing cells which were generated by sequentially infecting B-*myb*$^{f/f}$ MEFs cells with the Cre lentivirus and the WT B-Myb-encoding adenovirus (f/f:Cre+WT). The B-Myb-deficient cells and the M14-reexpressing cells took an unusually long time to complete mitosis, displayed marked difficulties in completing cytokinesis and had frequent defects in chromosome segregation (Fig. 11), although mitosis in the parental B-*myb*$^{f/f}$ cells appeared normal. In control experiments, reexpression of WT B-Myb suppressed the abnormalities seen in the B-Myb-deficient cells.

Consistent with these observations, the proportion of cells in mitosis (the mitotic index) increased 2.6 and 2.3 fold in the B-Myb-deficient cells and M14-reexpressing cells, respectively (WT MEFs, 5.0 $\pm$ 0.8%; f/f:Cre cells, 11.4 $\pm$ 2.4%; f/f:Cre+M14, 13.2 $\pm$ 1.8%) (Fig. 12A). We examined the proportion of cells at each stage of mitosis. B-Myb-deficient cell populations had significantly greater number of cells in prometaphase compared to wild-type cells ($P < 0.05$) (Fig. 12B). M14-reexpressing cells had slightly increased numbers of cells in metaphase compared to wild-type cells or WT-reexpressing cells, although the trends were not significant ($P = 0.1$ and $P = 0.115$, respectively). Thus, M14-reexpressing cells spent longer periods of time in metaphase compared to WT cells.

FACS analysis demonstrated that the M14-reexpressing cells and the B-Myb-deficient cells included readily detectable fractions of cells with chromosomal contents of 8N which were not evident in the WT MEFs or the WT B-Myb-reexpressing cells (Fig. 12C). We also quantified the number of centrosomes per cell in MEFs. About 70% of the M14-reexpressing cells had an abnormal number of centrosomes, approximately 1/3 had 4 centrosomes 1/6 had 3 centrosomes (Fig. 12D). In contrast, approximately 90% of parental MEFs and 70% of WT B-Myb reexpressing cells had 2 centrosomes. Thus, cells expressing M14 B-Myb instead of the normal B-Myb exhibited defects in mitosis and abnormalities in DNA content and centrosome number.

The M14-reexpressing MEFs and the B-Myb-deficient cells exhibited various mitotic abnormalities, which have also been observed in clathrin-depleted cells (Royle et al., 2005). The metaphase plate in the M14-reexpressing cells and the B-Myb-deficient cells was thicker than in parental MEFs and WT B-Myb-reexpressing cells (Fig. 13A, B) and there was an increased incidence of misaligned chromosomes in M14-reexpressing cells and the B-Myb-deficient cells (Fig. 13C). Misaligned chromosomes were observed in 53.3 $\pm$ 7.6% of the M14-reexpressing cells and in 55.4 $\pm$ 6.5% of the B-Myb-deficient cells, but only in 7.6 $\pm$ 2.7% of the WT B-Myb-reexpressing cells. In the M14-reexpressing cells and the B-Myb-deficient cells, misaligned chromosomes usually consisted of pairs of sister chromatids (Fig. 13D). After depolymerization of microtubules by cold treatment, M14-reexpressing cells and the B-Myb-deficient cells often contained centromeres that did not have a spindle fibres attached (Fig. 13E, arrowheads), suggesting that the stability of the kinetochore-spindle contacts was reduced. In WT B-Myb-reexpressing cells, Mad2 correctly localized to kinetochores at early prometaphase and then became diffusely distributed at metaphase (Fig. 13F), indicating that correct attachment of chromosomes to kinetochore fibres was monitored by the spindle checkpoint

(Cleveland et al., 2003). In contrast, in M14-reexpressing cells and the B-Myb-deficient cells, Mad2 was found on the kinetochores of misaligned chromosomes as well as chromosomes at the metaphase plate, indicating that the spindle checkpoint was still activated on properly aligned chromosomes. These results indicate that the primary cause of prolonged mitosis in M14-reexpressing cells was the continued activation of the spindle checkpoint, which resulted from destabilization of kinetochore microtubules.

DISCUSSION

B-Myb is the member most closely related to *Drosophila* Myb (dMyb) (David son et al., 2005). Mutants of d*myb* and zebrafish B-*myb* exhibit defects in cell cycle progression and genome instability (Katzen et al., 1998; Okada et al., 2002; Fung et al., 2002; Manak et al., 2002; Shepard et al., 2005). Furthermore, dMyb was recently shown to contribute to normal separation of centrosomes and also chromosome condensation (Goshima et al., 2007; Manak et al., 2007). However, it remains unknown whether these defects are mediated indirectly through its role in gene transcription or reflect a direct action of dMyb. In fact, B-Myb is required for transcription of a cluster of genes which regulate the G2/M transition and the M-phase events (Zhu et al., 2004; Osterloh et al., 2006; Pilkinton et al., 2007; Litovchick et al., 2007). The present study clearly demonstrates that the Myb-Clafi complex directly regulate the function of mitotic spindles. The B-Myb M14 mutant, which retains the capacity to activate transcription of a cluster of B-Myb target genes but cannot form the Myb-Clafi complex, induced the multiple defects of mitosis, including misaligned chromosomes and unusual number of centrosomes. To our knowledge, this is the first report indicating that the DNA-binding transcription factor directly regulates the function of the mitotic spindle.

B-Myb is known to form the vertebrate dREAM/Myb-MuvB-like complex (Zhu et al., 2004; Osterloh et al., 2006; Pilkinton et al., 2007; Litovchick et al., 2007). One obvious question is why other groups did not detect the Myb-Clafi complex when they analyzed the dMyb- or B-Myb-containing complex. This may be due to low amount of the Myb-Clafi complex compared to the dREAM/Myb-MuvB-like complex, because the Myb-Clafi complex exists only at the M-phase. Based on our results, we have estimated that the amount of the Myb-Clafi complex is less than 5% of the dREAM/Myb-MuvB-like complex. We have used the high-salt condition (0.42 M NaCl) to purify the Myb-Clafi complex, while the low-salt condition (0.1 M KCl) was used to purify the dREAM/Myb-MuvB complex (Korenjak et al., 2004; Lewis et al., 2004). By using the low-salt condition (150 mM NaCl), an interaction between B-Myb and hLIN-9 (a human homologue of Mip130) or other components of the human dREAM/Myb-MuvB-like complex was detected by co-immnoprecipitation (Osterloh et al., 2006; Litovchick et al., 2007). We have also observed that B-Myb can be co-precipitated with hLIN-9 (Fig. 5C) under the low-salt condition. Under the high-salt condition used to purify the Myb-Clafi complex, the dREAM/Myb-MuvB-like complex may be disrupted, which might disclose the presence of the Myb-Clafi compex.

Although we observed that B-Myb and clathrin signals were detected at the kinetochore fibres, clathrin signals were more resistant to detergent extraction (data not shown), suggesting that clathrin binds more tightly to the microtubules than B-Myb. This is consistent with previous work that detected clathrin, but neither B-Myb nor filamin, in the spindle apparatus (Mack and Compton, 2001). These data suggest that only CHC in the Myb-Clafi complex directly binds to the spindle with high affinity, or that the role of the Myb-Clafi complex is to deliver clathrin to the spindles. The estimated molecular weight of Myb-Clafi complex (500-600 kD) indicates that it consists of one molecule each of filamin A, CHC, CLC, and B-Myb. Clathrin can form a triskelion consisting of three heavy chains each with an associated light chain. However, the molecular weight of the Myb-Clafi complex suggests that clathrin does not form a triskelion in this complex. The recent report using the clathrin mutants suggested that the domains required for the trimer formation is critical for its function in mitotic spindles (Royle and Lagnado, 2006). These results also suggest that the Myb-Clafi complex delivers clathrin to the spindles, where clathrin forms triskelion. Alternatively, the domains in clathrin, which are required for trimer formation, could also be required for interaction with B-Myb and filamin to form the Myb-Clafi complex.

Clathrin is speculated to form a relatively rigid connection between microtubules that strengthens kinetochore fibres (Royle et al., 2005). Filamin is an actin crosslinking and molecular scaffold protein (Popowicz et al., 2006; Feng and Walsh, 2004) and B-Myb can also interact with various proteins (Ness, 1999). Therefore, both B-Myb and filamin may act as scaffold proteins to promote a connection between clathrin and microtubules, and possibly actin. We found that disruption of the Myb-Clafi complex causes aneuploidy, a form of genomic instability which leads to cancer (Jallepalli and Lengauer, 2001), suggesting that B-Myb acts as a tumor suppressor rather than an oncogene. Not only mutation and decreased expression, but also overexpression, of B-Myb may cause cancers by disrupting the Myb-Clafi complex due to an imbalance in the components. Identification and characterization of the Myb-Clafi complex may further our understanding of the role of B-Myb in mitotic events, as well as in cancer development.

EXPERIMENTAL PROCEDURES

Purification and Characterization of the Myb-Clafi Complex

To generate the retrovirus vector expressing FLAG- and HA-tagged B-Myb, the human B-*myb* cDNA was cloned into the pOZ-FH-N vector (Nakatani and Ogryzko, 2003). The generated retrovirus vector was transfected into the amphotropic packaging Phoenix A cells and medium containing the amphotropic virus was prepared. HeLa cells were transduced with a recombinant retrovirus expressing a bicistronic mRNA encoding the wild type or mutant form of FLAG-HA-B-Myb linked to the IL-2 receptor subunit, and the transduced subpopulation was purified by repeated cycles of affinity cell sorting. Cells were disrupted in hypotonic buffer (10 mM HEPES, pH 7.9, 1.5 mM $MgCl_2$, 10 mM KCl, 0.5 mM DTT), and the nuclear pellet was collected by centrifugation at 25,000 g for 20 min. The pellet was extracted with buffer C (20 mM HEPES, pH 7.9, 25% glycerol, 420 mM NaCl, 1.5 mM $MgCl_2$, 0.2 mM EDTA, 0.5 mM PMSF, 0.5 mM DTT) for 30 min at 4 °C and lysates were collected by centrifugation at 25,000 g for 30 min. The B-Myb complex was immunoprecipitated from nuclear extracts prepared from HeLa cells expressing B-Myb by incubating with M2 anti-FLAG agarose (Sigma) for 4 h with rotation. After an extensive wash with wash buffer (20 mM Tris-HCl, pH 8.0, 0.1 M KCl, 5 mM $MgCl_2$, 10% glycerol, 1 mM PMSF, 0.1% Tween 20, 10 mM β-mercaptoethanol), the bound proteins were eluted from the M2 agarose by incubation for 30 min with 0.2 mg/ml FLAG peptide (Sigma) in the same buffer. The eluates were further purified by immunoprecipitation with protein G-Sepharose (Amersham) conjugated to the anti-HA 12CA5 antibody. The bound proteins were eluted from the matrix by incubating for 60 min with 0.5 mg/ml HA peptide in wash buffer. The purified proteins was separated by 4–20% gradient SDS polyacrylamide gel electrophoresis (SDS–PAGE) and silver stained. For glycerol gradient sedimentation, 200 μl of FLAG antibody-immunoprecipitated material was loaded onto a 4.2 ml 10%–40% glycerol gradient in wash buffer. After centrifugation at 55,000 rpm for 5 h (Beckman, SW55Ti), 200 μl fractions were collected from the top of the gradient and resolved by 4-20% gradient SDS-PAGE and silver stained. The B-Myb complex fractions were TCA precipitated, resolved by 4-20% gradient SDS-PAGE and stained with Coomassie blue. Protein bands were excised and analyzed by mass spectrometry. Anti-B-Myb (N-19, Santa Cruz Biotech.), anti-filamin A (MAB1692, Chemicon), anti-CHC (X22, Affinity BioReagents), or anti-CLC (CON.1, Santa Cruz Biotech.) werte used for immunoblotting.

Culture and Transfection of HeLa Cells

HeLa cells were cultured in MEM supplemented with 10% calf serum (CS), 100 U/ml penicillin G sodium and 100 μg/ml streptomycin sulfate at 37 °C and in 5 % CO_2. HeLa cells (1 x 10^6 cells per 100-mm dish) were transfected with DNA plasmids (6 μg) using Lipofectamine Plus (Invitrogen) according to the manufacturer's instructions.

Synchronization of the Cell Cycle and FACS Analysis of HeLa Cells

HeLa cells (5 x 10^6 cells per 100-mm dish) were synchronized at the beginning of S phase using a double thymidine block and release protocol (20 h incubation with 2 mM thymidine, an interval of thymidine-free incubation for 8 h, and a second thymidine incubation for 14 h). Mitotic cells were collected by mechanical shake-off from the culture plate 8.5 h after release from S phase. For FACS analysis, HeLa cells were harvested, fixed with 70% ethanol, and DNA was stained with 25 μg/mL propidium iodide (Sigma). Cells were subjected to flow cytometry on a FACScan instrument (Becton Dickinson).

B-*myb* siRNA Treatment

The B-*myb* siRNA (GUUAAGAAGUAUGGCACAA) was designed to target human B-*myb*, according to the parameters of Tuschl and colleagues (Elbashir et al., 2001). The control siRNA (CGUACGCGGAAUACUUCGA) was designed to target luciferase. Duplex siRNA was synthesized with dTdT overhangs. HeLa cells (1 x 10^6 cells per 100-mm dish) were transfected with siRNAs using Oligofectamine (Invitrogen) according to the manufacturer's instructions. At various times after transfection, cells were used for lysate preparation or immunocytochemistry.

Co-immunoprecipitation

To examine the interaction between endogenous B-Myb and clathrin or filamin, Hela cells were lysed using buffer C for 30 min at 4 °C and the extracts were collected by centrifugation at 17,400 g for 10 min. The B-Myb complex was immunoprecipitated from the extracts by incubating with anti-B-Myb (N-19, Santa Cruz Biotech.) for 4 h with rotation, followed by incubating with protein G-Sepharose for 30 min. After five washes with wash buffer (20 mM Tris-HCl, pH 8.0, 0.1 M KCl, 5 mM $MgCl_2$, 10% glycerol, 1 mM PMSF, 0.1% Tween 20, 10 mM β-mercaptoethanol), the bound proteins were eluted by incubation for 30 min in 0.1 M glycine-HCl buffer (pH 2.5). The immuno-complexes were analyzed by SDS-PAGE, followed by Western blotting using anti-filamin A (MAB1692, Chemicon), anti-CHC (X22, Affinity BioReagents), and anti-B-Myb (N-19, Santa Cruz Biotech.). Co-immunoprecipitation using HeLa cells expressing FLAG/HA-B-Myb was performed as described in the B-Myb complex purification.

To examine the interaction between transiently expressed FLAG-B-Myb and endogenous clathrin or filamin, HeLa cells (1 x 10^6 cells per 100-mm dish) were transfected with the pact-FLAG-B-Myb WT, M14, or control vector (6 μg) using Lipofectamine Plus (Invitrogen) according to the manufacturer's instructions. Forty-eight

hours after transfection, cells were lysed and the extracts were collected as described above. The B-Myb complex was immunoprecipitated from the extracts by incubating with M2 anti-FLAG agarose (Sigma) for 4 h with rotation. After five washes with wash buffer, the bound proteins were eluted from M2 agarose by incubation for 30 min with 0.2 mg/ml FLAG peptide (Sigma) in the same buffer. The immuno-complexes were analyzed by SDS-PAGE, followed by Western blotting as described above.

To investigate the interaction between B-Myb and hLIN-9, HeLa cells (1 x 10^6 cells per 100-mm dish) were transfected with a mixture of the pact-FLAG-B-Myb WT, M14, or control vector (3 μg) and pcDNA3-HA-Lin-9 (3 μg) using Lipofectamine Plus (Invitrogen) according to the manufacturer's instructions. Forty-eight hours after transfection, cell lysates were prepared and used for coimmunoprecipitation with the anti-FLAG M2 antibody, according to the method described by Osterloh et al. (2006).

Immunocytochemistry

Cells were grown in 35 mm petri dishes. In the case of M-phase cells, cells were washed with 1% Triton X-100 in PBS for 1-10 min, and then fixed with 4% paraformaldehyde in phosphate-buffered saline (PBS) for 20 min at room temperature, as indicated in the Figure Legends. In the case of interphase cells, cells were permeabilized with 0.2% Triton X-100 treatment for 10 min after fixation. After incubation for 60 min with 3% skimmilk in PBS, cells were incubated for 1 h with the following primary antibodies: anti-GFP (598, Medical Biological Laboratories); anti-B-Myb (N-19 and H115, Santa Cruz Biotechnology); anti-CHC (X22, Affinity BioReagents); anti-α-tubulin (DM1A, Sigma); anti-CENPB (rabbit polyclonal, a gift from H. Masumoto) (Suzuki et al., 2004); phospho-histone H3 (Ser10) (06-570, Upstate); anti-E2F1 (H137, Santa Cruz Biotechnology); anti-E2F4 (C-20 and A-20, Santa Cruz Biotechnology); and anti-Aurora B (ab2254, Abcam). The cells were washed, incubated with Alexa Fluor 488- or Cy3- or Rhodamine-conjugated anti-rabbit or anti-mouse secondary antibodies (Molecular Probes or Chemicon). Chromatin was labeled with TOTO-3 iodide (Molecular Probes).

Microscopy

Confocal and Nomarski images were obtained using an LSM510 (Zeiss) laser scanning microscope. In order to minimize overlapping signals, images were obtained by sequential excitation at 488/543/633 nm, to detect Alexa Fluor 488, Cy3, and TOTO-3, respectively, and emission signals were detected at 505-530 nm for Alexa Fluor 488, >560 nm for Cy3, and >650 nm for TOTO-3 iodide. Images were processed using Photoshop software. Power output of the primary laser was checked regularly to ensure consistency (15 mW; anode current 3.3 A).

Quantitative immunostaining

For quantitative immunostaining experiments, identical laser power and acquisition settings were used. The mean pixel density of images was measured by LSM510 3.2 software at a depth of 8-bit. Spindle recruitment was assayed by dividing the mean pixel density measured in a 1 mm x 1 mm region of interest placed over the spindle ($F_{spindle}$) by that measured in a region outside the spindle ($F_{cytoplasm}$). Therefore, a value of one represents no specific localization at the spindles.

Metaphase plate thickness

The thickness of the metaphase plate was assessed by measuring the perpendicular distance between two limiting lines drawn parallel to the metaphase plate.

Mitotic index

The mitotic index was determined by counting the number of cells in mitosis as a fraction of the total number of cells within a 230 x 230 μm area. Cells from 5-6 independent experiments were counted. Mitotic cells were identified by the presence of condensed DNA and by phosphohistone H3 positive staining. Cells that expressed Cre recombinase were counted if they were Venus-positive. At least 100 cells were counted.

Analysis of Kinetochore-microtubles Attachments

GFP-a-tubulin was generated by PCR from a human spleen cDNA library (STRATAGENE) to introduce *Bgl*II and *Kpn*I sites and subcloned into pEGFP-C1 (Clontech). The GFP-a-tubulin fragment was cloned into the *Hpa* I site of the pDON-AI retroviral vector (Takara). To generate a GFP-a-tubulin retroviral vector, pDON-GFP-Tub was transfected using Lipofectamine 2000 (Invitrogen) according to the manufacturer's instructions into Platinum-E (Plat-E) packaging cells (Morita et al., 2000). Fifteen micrograms of pDON-GFP-Tub was transfected per 5 x 10^6 cells in a 10-cm plate. Three hours after transfection, the medium was removed and replaced with 10 ml of medium. After 24 h, the medium was removed and replaced with 6 ml of fresh medium and the plate was transferred to 32 °C. Supernatants were pooled 24 h after the last medium change. MEFs were infected with retrovirus to express GFP-a-tubulin with 8 μg/ml polybrane. Four hours after infection, cells were reinfected with lentivirus to express Cre recombinase, and then with adenoviruses to express B-Myb and M14-B-Myb, as described above. Cells were incubated at 4 °C for 10 min before fixation to depolymerize all non-kinetochore microtubules.

Quantification and Statistics

For image quantification and counting experiments, 10-50 cells were analysed, and 100-411 cells were counted, from 3-6 independent experiments. Results were analyzed in Microsoft Excel 2004 (Microsoft) and StatView-J-5.0 (SAS Institute Inc.) and figures were assembled in Adobe Photoshop 7.0. Results are expressed as mean ± S.D. Binomial results (mitotic index, misaligned chromosomes, multinucleate cells, etc.) were tested for approximation to a normal distribution and *P*-values were retrieved in StatView-J-5.0.

Long-term Imaging

Cells were cultured in poly-D-lysine coated glass bottom 35 mm dishes (IWAKI). For observation of living cells, medium was replaced with fresh DMEM containing 20 mM HEPES (pH 7.4). Dishes were imaged at 37 °C using a Tempcontrol 37-2 chamber (Zeiss). Images were obtained using an LSM510 (Zeiss) laser scanning microscope. Images were captured at set time intervals for a period of at least 6 h. Images were processed using the Zeiss LSM image software.

Generation of HeLa Cells Expressing Venus-B-Myb or EGFP-CLC

The retrovirus construct to express the B-Myb fusion protein with Venus, a GFP derivative (Nagai et al., 2002), was constructed using the pOZ-FH-N vector (Nakatani and Ogryzko, 2003) after removal of the FLAG-HA tag, and the virus was prepared as described above. HeLa cells expressing Venus-B-Myb were selected as described above. The vector to express EGFP-CLC was a kind gift from Dr. S. J. Royle (Royle et al., 2005). HeLa cells were transfected with this vector together with the plasmid to express neomycin-resistance marker, and G418-resistant cells were selected in the presence of medium containing 500 mg/ml G418.

Generation of B-*myb* Conditional Knockout Mice.

1) Construction of the Targeting Vector

Mouse B-*myb* genomic clones were isolated from a library derived from C57BL/6 mice by the standard plaque hybridization procedure. A 15.0 kb genomic DNA subfragment which contains the five exons encoding amino acids 8-200 was used to generate the targeting vector. The 5' loxP site was cloned in the appropriate orientation into the *Bgl*II site upstream of exon 5. A neomycin resistance cassette driven by the *PGK* promotor and flanked by loxP sequences was subcloned into the *Nco*I site upstream of exon 6. To enable negative selection against nonhomologous recombinants, a diphtheria toxin gene cassette (DT-A) (Yagi et al., 1993) was subcloned into the end of the targeting sequence.

2) Targeting of ES Cells and Generation of Conditional Knockout Mice

A *Not*I-linearized targeting vector (100 μg) was introduced into 2 x 10^7 TT2 ES cells by electroporation. Targeted clones were isolated after growth in the presence of G418 (150 μg/ml) for 7 days and were then expanded in 24-well plates. Homologous recombination was confirmed by Southern blot analysis using two different probes (a 5' probe and a 3' probe). To remove the neomycin cassette, Cre recombinase was expressed by transient transfection with the pac-Cre vector, in which the Cre cDNA was driven by the chicken cytoplasmic b-actin promoter. After removal of the neomycin cassette, targeted ES cells were injected into 8-cell embryos and standard procedures were followed to generate homozygous mice with the floxed allele.

Culture of Mouse Embryonic Fibroblasts (MEFs)

MEFs were prepared from E14.5 embryos with a genetic background >98% C57BL/6. Embryos from which the head and internal organs were removed were cut in pieces, and stirred in 0.1% trypsin for 30 min to isolate MEFs. MEFs were maintained in DMEM containing 10% fetal bovine serum (FBS) and 100 U/ml penicillin-streptomycin at 37 °C and 5% CO_2.

Generation of MEFs Expressing M14 Instead of Endogenous B-Myb

B-*myb*$^{f/f}$ MEFs were infected with lentivirus at an MOI of 10 for 12 h to express the Cre recombinase. Twelve hours after infection of lentivirus, cells were infected at an MOI of 5 with adenovirus to express M14 or WT B-Myb. All analyses were performed at 72 h after lentivirus infection. The vectors to generate lentivirus to express Cre recombinase were provided by H. Miyoshi (RIKEN BioResource Center: see URL: http://www.brc.riken.jp/lab/cfm/ for details). The construction of adenovirus expressing WT or M14 B-Myb used the Adenovirus Cre/loxP Kit Version 2.0, according to the manufacturer's instructions (BD Bioscience).

Analysis of B-Myb Target Gene Expression

Total RNA was isolated from MEFs using RNAeasy spin columns according to the manufacturer's instructions (Qiagen). The primers and probes were designed using the Primer Express software (Applied Biosystems) and are indicated in Table S1. Real-time RT-PCR was performed using the ABI 7500 Real-Time PCR System and QuantiTect Probe RT-PCR Kit (Qiagen) according to the manufacturer's instructions. The thermal cycling parameters were 50 °C for 30 min, 95 °C for 10 min, and 40 cycles of 95 °C for 15 sec, and 60 °C for 1 min. Data were collected and analyzed using the 7500 SDS system software (version 1.2.2; Applied Biosystems). The relative levels of transcripts for each gene in wild-type and mutant samples were compared following normalization to endogenous control targets, which were detected using Ribosomal RNA Control Reagents (VIC probe) (Applied Biosystems).

ACKNOWLEDGMENTS

We are grateful T. Takagai for his help, Y. Nakatani for the pOZ-FH-N vector, the staff of the Research Resources Center of the RIKEN Brain Science Institute for mass spectrometric analysis, H. Masumoto for the anti-CENPB antibody, S. J. Royle for the EGFP-CLC expression vector, S. Gaubatz for the HA-hLIN9 expression vector, A. Miyawaki for the Venus expression vector, H. Miyoshi for the lentivirus encoding Cre, and members of the Experimental Animal Division of the RIKEN Tsukuba Institute for maintenance of the mice. This work was supported by Grants-in-aid for Scientific Research and by grant from the Genome Network Project of the Ministry of Education, Culture, Sports, Science and Technology of Japan.

REFERENCES

Beall, E.L., Bell, M., Georlette, D., and Botchan, M.R. (2004). Dm-*myb* mutant lethality in Drosophila is dependent upon mip130: positive and negative regulation of DNA replication. Genes Dev. *18,* 1667-1680.

Beall, E.L., Manak, J.R., Zhou, S., Bell, M., Lipsick, J.S., and Botchan, M.R. (2002). Role for a *Drosophila* Myb-containing protein complex in site-specific DNA replication. Nature *420,* 833-837.

Bender, T.P., Kremer, C.S., Kraus, M., Buch, T., and Rajewsky, K. (2004). Critical functions for c-Myb at three checkpoints during thymocyte development. Nature Immunol. *5,* 721-729.

Bessa, M., Saville, M.K., and Watson, R.J. (2001). Inhibition of cyclin A/Cdk2 phosphorylation impairs B-Myb transactivation function without affecting interactions with DNA or the CBP coactivator. Oncogene *20,* 3376-3386.

Ceol, C.J., Stegmeier, F., Harrison, M.M., and Horvitz, H.R. (2006). Identification and classification of genes that act antagonistically to let-60 Ras signaling in Caenorhabditis elegans vulval development, Genetics *173,* 709–726.

Cleveland, D.W., Mao, Y., and Sullivan, K.F. (2003). Centromeres and kinetochores: from epigenetics to mitotic checkpoint signaling. Cell *112,* 407-421.

Dai, P., Akimaru, H., Tanaka, Y., Hou, D.-X., Yasukawa, T., Kanei-Ishii, C., Takahashi, T., and Ishii, S. (1996). CBP as a transcriptional coactivator of c-Myb. Genes Dev. *10,* 528-540.

Davidson, C., Tirouvanziam, R., Herzenberg, L., and Lipsick, J. (2005). Functional evolution of the vertebrate *myb* gene family: B-Myb, but neither A-Myb nor c-Myb, complements *Drosophila* Myb in hemocytes. Genetics *169,* 215-229.

Edeling, M. A., Smith, C., and Owen, D. (2006). Life of a clathrin coat: insights from clathrin and AP structures. Nature Rev. Mol. Cell. Biol. *7,* 32-44.

Elbashir, S.M., Harborth, J., Lendeckel, W., Yalcin, A., Weber, K., and Tuschl, T. Duplexes of 21-nucleotide RNAs mediate RNA interference in cultured mammalian cells. Nature *411,* 494-498.

Enari, M., Ohmori, K., Kitabayashi, I., and Taya, Y. (2006). Requirement of clathrin heavy chain for p53-mediated transcription. Genes Dev. *20,* 1087-1099.

Fay, D.S., and Han, M. (2000). The synthetic multivulval genes of *C. elegans*: functional redundancy, Ras-antagonism, and cell fate determination, Genesis *26,* 279–284.

Feng, Y., and Walsh, C.A. (2004). The many faces of filamin: a versatile molecular scaffold for cell motility and signalling. Nature Cell Biol. *6,* 1034-1038.

Fung, S.M., Ramsay, G., and Katzen, A.L. (2002). Mutations in *Drosophila myb* lead to centrosome amplification and genomic instability. Development *129,* 347-359.

Gonda, T.J., and Metcalf, D. (1984). Expression of myb, myc and fos proto-oncogenes during the differentiation of a murine myeloid leukaemia. Nature 310, 249-251.

Goshima, G., Wollman, R., Goodwin, S.S., Zhang, N., Scholey, J.M., Vale, R.D., and Stuurman, N. (2007). Genes required for mitotic spindle assembly in *Drosophila* S2 cells. Science *316,* 417-421.

Harrison, M.M., and Ceol, C.J., Lu, X., and Horvitz, H.R. (2006). Some *C. elegans* class B synthetic multivulva proteins encode a conserved LIN-35 Rb-containing complex distinct from a NuRD-like complex, Proc. Natl. Acad. Sci. USA *103,* 16782–16787.

Jallepalli, P.V., and Lengauer, C. (2001). Chromosome segregation and cancer: cutting through the mystery. Nature Rev. Cancer *1,* 109-117.

Katzen, A.L., Jackson, J., Harmon, B.P. Fung, S.M., Ramsay, G., and Bishop, J.M. (1998). *Drosophila myb* is required for the G2/M transition and maintenance of diploidy. Genes Dev. *12,* 831-843.

Korenjak, M., Taylor-Harding, B., Binné, U.K., Satterlee, J.S., Stevaux, O., Aasland, R., White-Cooper, H., Dyson, N., and Brehm A. (2004). Native E2F/RBF complexes contain Myb-interacting proteins and repress transcription of developmentally controlled E2F target genes. Cell *119,* 181-193.

Lewis, P.W., Beall, E.L., Fleischer, T.C., Georlette, D., Link, A.J., and Botchan, M.R. (2004). Identification of a *Drosophila* Myb-E2F2/RBF transcriptional repressor complex. Genes Dev. *18,* 2929-2940.

Litovchick, L., Sadasivam, S., Florens, L., Zhu, X., Swanson, S.K., Velmurugan, S., Chen, R., Washburn, M.P.,

Liu, X.S., and DeCaprio, J.A. (2007). Evolutionarily conserved multisubunit RBL2/p130 and E2F4 protein complex represses human cell cycle-dependent genes in quiescence. Mol. Cell *26,* 539-551.

Mack, G.J., and Compton, D.A. (2001). Analysis of mitotic microtubule-associated proteins using mass spectrometry identifies astrin, a spindle-associated protein. Proc. Natl. Acad. Sci. USA *98,* 14434-1449.

Manak, J.R., Mitiku, N., and Lipsick, J.S. (2002). Mutation of the *Drosophila* homologue of the Myb protooncogene causes genomic instability. Proc. Natl. Acad. Sci. USA *99,* 7438-7443.

Manak, J.R., Wen, H., Van, T., Andrejka, L., and Lipsick, J.S. (2007). Loss of *Drosophila* Myb interrupts the progression of chromosome condensation. Nature Cell Biol. *9,* 581-587.

Morita, S., Kojima, T., and Kitamura, T. (2000). Plat-E: an efficient and stable system for transient packaging of retroviruses. Gene Ther. *7,* 1063-1066.

Mucenski, M.L., McLain, K., Kier, A.B., Swerdlow, S.H., Schereiner, C.M., Miller, T.A., Pietryga, D.W., Scott, W.J., and Potter, S.S. (1991). A functional c-*myb* gene is required for normal murine fetal hepatic hematopoiesis. Cell *65,* 677-689.

Nagai, T., Ibata, K., Park, E.S., Kubota, M., Mikoshiba, K., and Miyawaki. A. (2002). A variant of yellow fluorescent protein with fast and efficient maturation for cell-biological applications. Nature Biotechnol. *20,* 87-90.

Nakagoshi, H., Takemoto, Y., and Ishii, S. (1993). Functional domains of the human B-*myb* gene product. J. Biol. Chem. *268,* 14161-1417.

Nakatani, Y., and Ogryzko, V. (2003). Immunoaffinity purification of mammalian protein complexes. Methods Enzymol. *370,* 430-444 .

Ness, S.A. (1999). Myb binding proteins: regulators and cohorts in transformation. Oncogene *18,* 3039-3046.

Nomura, N., Takahashi, M., Matsui, M., Ishii, S., Date, T., Sasamoto, S., and Ishizaki, R. (1988). Isolation of human cDNA clones of *myb*-related genes, A-*myb* and B-*myb*. Nucleic Acids Res. *16,* 11075-11089.

Ogata, K., Morikawa, S., Nakamura, H., Sekikawa, A., Inoue, T., Kanai, H., Sarai, A., Ishii, S., and Nishimura, Y. (1994). Solution structure of a specific DNA complex of the Myb DNA-binding domain with cooperative recognition helices. Cell *79,* 639-648.

Oh, I.H., and Reddy, E.P. (1999). The *myb* gene family in cell growth, differentiation and apoptosis. Oncogene *18,* 3017-3033.

Okada, M., Akimaru, H., Hou, D.-X., Takahashi, T., and Ishii, S. (2002). Myb controls G2/M progression by inducing cyclin B expression in the *Drosophila* eye imaginal disc. EMBO J. *21,* 675-684.

Okamoto, C.T., McKinney, J., and Jeng, Y.Y. (2000). Clathrin in mitotic spindles. *Am.* J. Physiol. Cell. Physiol. *279,* C369-374.

Osterloh, L., von Eyss, B., Schmit, F., Rein, L., Hübner, D., Samans, B., Hauser, S., and Gaubatz, S. (2006). The human synMuv-like protein LIN-9 is required for transcription of G2/M genes and for entry into mitosis. EMBO J. *26,* 144-157.

Pilkinton, M., Sandoval, R., Song, J., Ness, S..A, and Colamonici, O.R. (2007). Mip/LIN-9 regulates the expression of B-Myb and the induction of cyclin A, cyclin B, and CDK1. J. Biol. Chem. *282,* 168-175.

Popowicz, G.M., Schleicher, M., Noegel, A.A., and Holak TA. (2006). Filamins: promiscuous organizers of the cytoskeleton. Trends Biochem. Sci. *31,* 411-419.

Robinson, C., Light, Y., Groves, R., Mann, D., Marias, R., and Watson, R. (1996). Cell-cycle regulation of B-Myb protein expression: specific phosphorylation during the S phase of the cell cycle. Oncogene *12,* 1855-1864.

Royle, S.J., Bright, N.A., and Lagnado, L. (2005). Clathrin is required for the function of the mitotic spindle. Nature *434,* 1152-1157.

Royle, S.J., and Lagnado, L. (2006). Trimerisation is important for the function of clathrin at the mitotic spindle. J. Cell Sci. *119,* 4071-4078.

Sakura, H., Kanei-Ishii, C., Nagase, T., Nakagoshi, H., Gonda, T.J., and Ishii, S. (1989). Delineation of the three functional domains of the transcriptional activator encoded by the c-*myb* protooncogene. Proc. Natl. Acad. Sci. USA *86,* 5758-5762.

Shepard, J.L., Amatruda, J.F., Stern, H.M., Subramanian, A., Finkelstein, D., Ziai, J., Finley, K.R., Pfaff, K.L., Hersey, C., Zhou, Y., Barut, B., Freedman, M., Lee, C., Spitsbergen, J., Neuberg, D., Weber, G., Golub, T.R., Glickman, J.N., Kutok, J.L., Aster, J.C., and Zon, L.I. (2005). A zebrafish *bmyb* mutation causes genome instability and increased cancer susceptibility. Proc. Natl. Acad. Sci. USA *102,* 13194-13199.

Suzuki, N., Nakano, M., Nozaki, N., Egashira, S., Okazaki, T., and Masumoto H. (2004). CENP-B interacts with CENP-C domains containing Mif2 regions responsible for centromere localization. J. Biol. Chem. *279,* 5934-5946

Tanaka, Y., Patestos, N.P., Maekawa, T., and Ishii, S. (1999). B-*myb* is required for inner cell mass formation at an early stage of development. J. Biol. Chem. *274,* 28067-28070.

Trauth, K., Mutschler, B., Jenkins, N.A., Gilbert, D.J., Copelend, N.G. and Klempnauer, K.-H. (1994). Mouse A-myb encodes a trans-activator and is expressed in mitotically active cells of the developing central nervous system, adult testis and B lymphocytes. EMBO J. *13,* 5994-6005

Toscani, A., Mettus, R.V., Coupland, R., Simpkins, H., Letvin, J., Orth, J., Hatton, K.S. and Reddy, E.P. (1997). Arrest of spermatogenesis and defective breast development in mice lacking A-*myb*. Nature *386,* 713-717

Yagi, T., Nada, S., Watanabe, N., Tamemoto, H., Kohmura, N., Ikawa, Y., and Aizawa, S. (1993). A novel negative selection for homologous recombinants using diphtheria toxin A fragment gene. Anal. Biochem. *214,* 77-86.

Zhu, W., Giangrande, P.H., and Nevins, J.R. (2004). E2Fs link the control of G1/S and G2/M transcription. EMBO J. *23,* 4615-4626.

Figure Legends

Figure 1. Purification of the B-Myb-Clafi Complex
(A) Generation of HeLa S3 cell lines expressing FLAG/HA-B-Myb. Whole cell lysates from the parental HeLa S3 cell line and two cell lines generated by infection with the retrovirus encoding FLAG/HA-B-Myb were used for Western blotting with an anti-B-Myb antibody.
(B) Purification of the B-Myb complex. The B-Myb complex was immunopurified using anti-FLAG and anti-HA antibodies from nuclear extracts of HeLa cells expressing FLAG/HA-B-Myb, resolved by SDS-PAGE, and visualized by silver staining. Two high molecular weight bands in addition to the FLAG-HA-B-Myb are indicated by the arrowheads.

Figure 2. Identification of the Myb-Clafi Complex
(A) Analysis of the Myb-Clafi complex by glycerol gradient centrifugation. The B-Myb complex was immunopurified from HeLa cells expressing FLAG/HA-tagged B-Myb using anti-FLAG. The immunopurified complex was separated on a 10%-40% glycerol gradient by ultracentrifugation, resolved by SDS-PAGE, and visualized by silver staining. The polypeptides identified by mass spectrometric analysis are indicated.
(B) Immunoblotting of the Myb-Clafi complex. The glycerol gradient purified B-Myb complex was analyzed by immunoblotting with the indicated antibodies.

Figure 3. Cell Cycle Synchronization of HeLa Cells
HeLa cell cycling was blocked at the G1/S boundary by a double thymidine block protocol, and cells were then analyzed by fluorescence activated cell sorting (FACS) at various times after release from the G1/S block.

Figure 4. Myb-Clafi Complex Is Abundant in the M-phase Cells
(A) Levels of B-Myb during the cell cycle. Whole cell lysates were prepared from HeLa cells at various times after release from the G1/S block, and used for Western blotting with the anti-B-Myb antibody.
(B) Co-immunoprecipitation of FLAG/HA-B-Myb with clathrin and filamin A. HeLa cells expressing FLAG/HA-B-Myb (FH-B-Myb) or no epitope-tagged protein (Mock) were synchronized by double thymidine block, and subsequently released from the G1-S boundary. At the indicated times after release, cells were lysed and separated into nuclear and cytosolic fractions. Cytosolic (left panels) and nuclear (right panels) fractions were immunoprecipitated with anti-FLAG, and the precipitates were subjected to immunoblot analysis with the antibodies indicated on the left.
(C) Co-immunoprecipitation of endogenous B-Myb with clathrin and filamin A. The G2/M-phase-enriched (G2/M) or unsynchronozed (Unsyn.) parental HeLa cells were lysed and cytosolic fractions were immunoprecipitated with anti-B-Myb or control IgG, and the precipitates were subjected to immunoblot analysis to detect the proteins with the antibodes indicated on the right.

Figure 5. Localization of B-Myb at the Kinetochore Fibres
(A) Localization of endogenous B-Myb during the cell cycle. HeLa cells were synchronized, washed with (for metaphase cells) or without (for interphase cells) 1% Triton X-100 prior to fixation, and subjected to indirect immunofluorescent staining with anti-B-Myb antibodies (Alexa Fluor 488, green) and anti-α-tubulin (Cy3, red), and visualized using confocal microscopy. DNA was stained with TOTO-3 iodide (blue). Cells were staged on the basis of the distribution of chromosomes. Scale bars: 10 μm.
(B) HeLa cells expressing Venus-B-Myb were synchronized, washed with or without Triton X-100 prior to fixation as described above, and subjected to indirect immunofluorescent staining with anti-GFP (Alexa Fluor 488, green), α-tubulin (red) and DNA (blue) were visualized as described above. Scale bars: 10 μm.

Figure 6. Detection of B-Myb and E2F1/4 on Condensed Chromosomes During Mitosis Using Weak Detergent Extraction Condition
(A) Detection of B-Myb on condensed chromosomes during mitosis using weak detergent extraction condition. HeLa cells expressing Venus-B-Myb were synchronized by the double thymidine block protocol, and released from the G1-S boundary. Cells were washed with 1% Triton X-100 for 1 min, fixed, and subjected to indirect immunofluorescent staining with anti-GFP antibodies (Alexa Fluor 488, green) and anti-α-tubulin (Cy3, red), and TOTO-3 iodide staining (blue) for DNA, and visualized using confocal microscopy. Cells were staged on the basis of the distribution of chromosomes. Scale bars: 10 μm.
(B) Detection of E2F1/4 on condensed chromosomes. HeLa cells were synchronized, washed with 1% Triton

X-100 for 5 min, fixed, and stained with anti-E2F1/4 (Alexa Fluor 488, green), anti-α-tubulin (Cy3, red), and TOTO-3 iodide staining (blue), as described above. Scale bars: 10 μm.

Figure 7. The Effect of B-Myb Depletion on the Mitotic Events of HeLa Cells
(A) Down-regulation of B-Myb by siRNA. Whole cell lysates were prepared from HeLa cells transfected with B-*myb* siRNA or control luciferase siRNA, and used for Western blotting with antibodies to detect the proteins indicated on the right.
(B) Defects in mitosis in B-Myb-depleted cells. Selected video frames from a time-lapse recording of M-phase cells treated with B-*myb* siRNA or control siRNA. Seven representative pictures derived from a 2 h time course are shown. The mitotic cells are indicated by white arrows.

Figure 8. Decrease in B-Myb Reduces Clathrin on the Mitotic Spindles and Leads to Mitotic Arrest
(A) Decrease in B-Myb reduces clathrin signals on the mitotic spindles. HeLa cells were treated with a control luciferase siRNA (upper panels) or B-*myb* siRNA (lower panels), subjected to indirect immunofluorescent staining with anti-clathrin HC (Cy3, red), and anti-α-tubulin (Alexa Fluor 488, green). DNA was stained with TOTO-3 iodide (blue) and cells were visualized using confocal microscopy. Scale bars: 10 μm. On the right, the clathrin signal at the mitotic spindle was quantified and indicated by bar graph with ± SD. **, $P < 0.01$. A value of one represents no specific signal at the mitotic spindle (see Experimental Procedures).
(B) B-Myb depletion decreased clathrin light chain (CLC) signals localization to the mitotic spindle. HeLa cells expressing EGFP-CLC were isolated, and were then transfected with B-*myb* siRNA or control luciferase siRNA. Cells were exatracted with 1% Triton X-100 for 10 min prior to fixation, and immunostained with anti-GFP and visualized using confocal microscopy. Scale bars: 10 mm.
(C) B-Myb depletion enhances mitotic arrest. The mitotic incidence of HeLa cells transfected with B-*myb* siRNA or control luciferase siRNA are indicated in the bar graph.
(D and E) B-Myb depletion caused thicker metaphase plates and an increase in misaligned chromosomes. HeLa cells transfected with B-*myb* siRNA or control luciferase siRNA were fixed, washed with 0.2% Triton X-100 for 10 min, and immunostained with anti-Aurora B or anti-CENPB (Cy3, red), anti-α-tubulin (Alexa Fluor 488, green), and TOTO-3 iodide (blue), and visualized using confocal microscopy. A typical example is shown. The misaligned chromosomes (arrow) and thickness of the metaphase plates are indicated. Scale bars: 10 μm.

Figure 9. The B-Myb Mutant M14 Retains its *trans*-Activation Capacity but Cannot Form the Myb-Clafi Complex
(A) Structures of WT and M14 B-Myb are shown schematically.
(B) M14 interacts with neither clathrin nor filamin A. HeLa cells were transfected with the FLAG/HA-tagged WT or M14 B-Myb expression plasmid, and whole cell lysates were used for coimunoprecipitation with anti-FLAG, followed by Western blotting to detect the proteins indicated on the left.
(C) M14 can bind to hLIN-9. HeLa cells were co-transfected with a FLAG-tagged WT or M14 B-Myb expression plasmid and a HA-hLIN-9 expression plasmid, and nuclear extracts were used for coimunoprecipitation with anti-FLAG, followed by Western blotting to detect the proteins indicated on the left.
(D) Preparation of MEFs expressing M14 instead of endogenous B-Myb. Whole cell lysates were prepared from the cells, and subjected to Western blotting using anti-B-Myb, anti-Cre, or anti-a-tubulin, as indicated. +/+, WT MEFs; f/f, B-$myb^{f/f}$ MEFs; f/f:CRE, B-$myb^{f/f}$ MEFs infected with the lentivirus encoding Cre recombinase; f/f:Cre+M14 and f/f:Cre+WT, B-$myb^{f/f}$ MEFs infected with the lentivirus encoding Cre recombinase, and then infected with the adenovirus to express FLAG/HA-tagged M14 and WT B-Myb, respectively.
(E) M14 can *trans*-activate B-Myb target genes. RNA was prepared from the indicated cells and the mRNA levels of seven B-Myb target genes were measured using real-time RT-PCR (n = 6). The mRNA levels of all seven genes in the f/f:Cre cells were significantly lower than levels in the other three cell types (*, $P < 0.05$).
(F) Reduction of clathrin at the mitotic spindles in M14-reexpressing cells. The indicated MEFs were subjected to indirect immunofluorescent staining with anti-clathrin HC (Cy5, red) and anti-α-tubulin (FITC, green), and visualized using confocal microscopy. DNA was visualized by staining with propidium iodide (blue). Scale bars: 5 μm. On the right, the clathrin signal at the mitotic spindle was quantified and indicated by bar graph with ± SD. *, $P < 0.05$. A value of one represents no specific signal at the mitotic spindle (see Experimental Procedures).

Figure 10. Generation of a B-*myb* Conditional Knockout Allele
(A) Schematic representation of the targeting vector, the wild-type, modified (fNeo), floxed (f), and deleted (-), B-*myb* alleles. LoxP sites (red arrow heads) and a PGK-neoR cassette, flanked by loxP sites, were introduced into the B-*myb* gene by homologous recombination to produce the B-*myb* modified allele (fNeo). Exons are represented by rectangles. B: *Bgl*II, Bs: E: *Eco*RI, EV: *Eco*RV, N: *Nco*I, S: *Sac*I, P: *Pst*I (Note: only one *Pst*I site is shown here among multiple *Pst*I sites).
(B) Targeted events were detected by Southern blot analysis of genomic DNA from ES cells. *Eco*RV-digested DNAs were hybridized to the external 5'-probe: a 6.4 kbp band was observed for the wild-type allele, a 10.0 kbp band for the fNeo allele, and an 11.3 kbo band for the floxed allele. *Nco*I-digested DNAs were hybridized to the external 3'-probe: an 8.0-kbp band was observed for the wild-type allele and an 8.6 kbp band for the fNeo allele.

To generate the floxed (f) allele, ES cells containing the fNeo allele were transfected with the Cre recombinase expression plasmid (pact-Cre). The presence of the loxP sites in the fNeo and floxed alleles was confirmed by DNA sequencing using the appropriate primers.
(C) Mice were generated by blastocyst injection of ES cells containing the floxed allele, and the MEFs were prepared from the heterozygous and homozygous floxed mice. The presence of the two loxP sites in the targeted cells was confirmed by PCR analysis. The BMlox1 and BMlox2 primers produce fragments of 125 bp and 213 bp from the wild type and loxP-containing alleles, respectively.
(D) To generate the deleted allele, MEFs were infected with the lentivirus encoding Cre recombinase. Primers BMlox2 and BMlox3 produce a fragment of 310 bp when sequences between the two loxP sites have been deleted (lower panel), while they generate a fragment of 3200 bp from the wild-type or floxed allele.

Figure 11. Defects in Mitosis of the M14-reexpressing Cells
Selected video frames are shown from a time-lapse recording of wild-type MEFs (+/+), MEFs in which B-*myb* was disrupted (f/f:Cre), MEFs reexpressing exogenous M14 (f/f:Cre+M14), or reexpressing wild-type B-Myb (f/f:Cre+WT) instead of endogenous B-Myb. Five representative pictures derived from the indicated time courses (min) are shown. Scale bar, 15 μm.

Figure 12. The B-Myb M14 Mutant Delays Mitosis and Causes Aneuploidy
(A) Increase in mitotic index in the M14-reexpressing cells and the B-Myb-deficient cells. The mitotic index of MEFs from the above experiments is shown. n = 235-589. *, $P<0.05$.
(B) The histogram shows the percentage of mitotic cells, relative to controls, at each stage in mitosis. Values are mean + SEM. **, $P<0.001$; *, $P<0.05$. n = 300.
(C) Multiploidy in M14-reexpressing cells and the B-Myb-deficient cells. The indicated cell types were analyzed by FACS (n=3).
(D) Abnormal numbers of centrosomes in M14-reexpressing cells and the B-Myb-deficient cells. The number of centrosomes was examined by immunostaining with anti-g-tubulin. *, $P<0.05$. n = 120.

Figure 13. The Myb-Clafi Complex Is Required for Function of the Mitotic Spindle
(A) Thicker metaphase plates in M14-reexpressing cells and the B-Myb-deficient cells. The indicated MEFs were immuno-stained with anti-α-tubulin (red). DNA was stained with TOTO-3 (blue). Cells expressing Cre recombinase together with Venus were immunostained with anti-GFP (green). Signals were visualized with appropriate secondary antibodies using confocal microscopy. Scale bars: 5 μm.
(B) Increased thickness of the metaphase plate in M14-reexpressing cells and the B-Myb-deficient cells. The thickness of the metaphase plate ± SD (n = 30) is shown. **, $P < 0.001$.
(C) Increase in misaligned chromosomes in M14-reexpressing cells and the B-Myb-deficient cells. The frequency of metaphase-like cells with misaligned chromosomes ± SD (n = 100-120) is shown.
(D) Misaligned chromosomes in M14-reexpressing cells and B-Myb-deficient cells were pairs of sister chromatids. Cells were stained with anti-CENPB (red) and anti-phospho-histon H3 antibody (blue). Misaligned chromosomes were not obviously detected in the wild-type control (+/+) cells. Scale bars: 5 μm.
(E) Failure in attachment of kinetochores to microtubules in M14-reexpressing cells and B-Myb-deficient cells. The indicated cells were stained for CENPB (red) and a-tubulin (green), after cold treatment to depolymerize non-kinetochore microtubules. The right panels show higher magnification images of the centromeres delineated by the white box. The arrows indicate the centromeres which are normally connected with a-tubulin, while the arrowheads indicate the centromeres which are not connected with a-tubulin. Scale bars: 5 μm.
(F) Persistent localization of Mad2 on kinetochores of M14-reexpressing cells and B-Myb-deficient cells. Cells were stained with anti-Mad2 (red) and anti-phospho-histon H3 (blue). The right panels show higher magnification images of the kinetochores delineated by the white box. Mad2-positive kinetochores are indicated by the arrowheads. Scale bars: 5 μm.

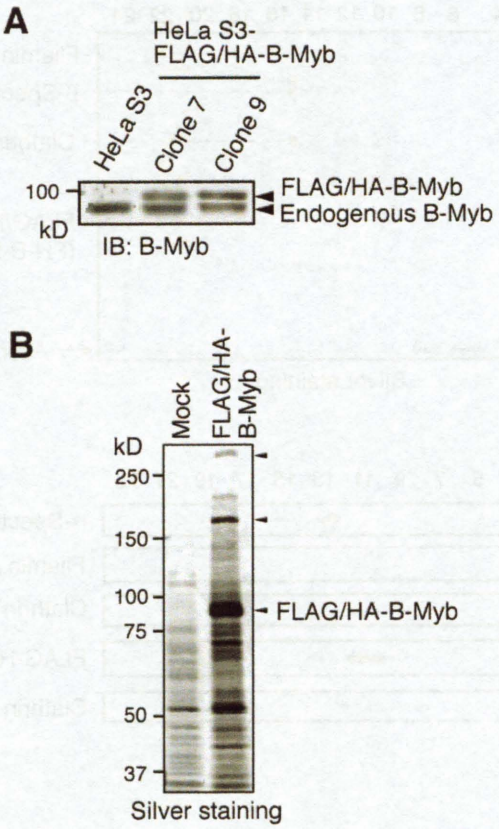
A
HeLa S3-
FLAG/HA-B-Myb
HeLa S3
Clone 7
Clone 9
100
kD
FLAG/HA-B-Myb
Endogenous B-Myb
IB: B-Myb
B
Mock
FLAG/HA-
B-Myb
kD
250
150
100
75
50
37
FLAG/HA-B-Myb
Silver staining

Fig. 1.

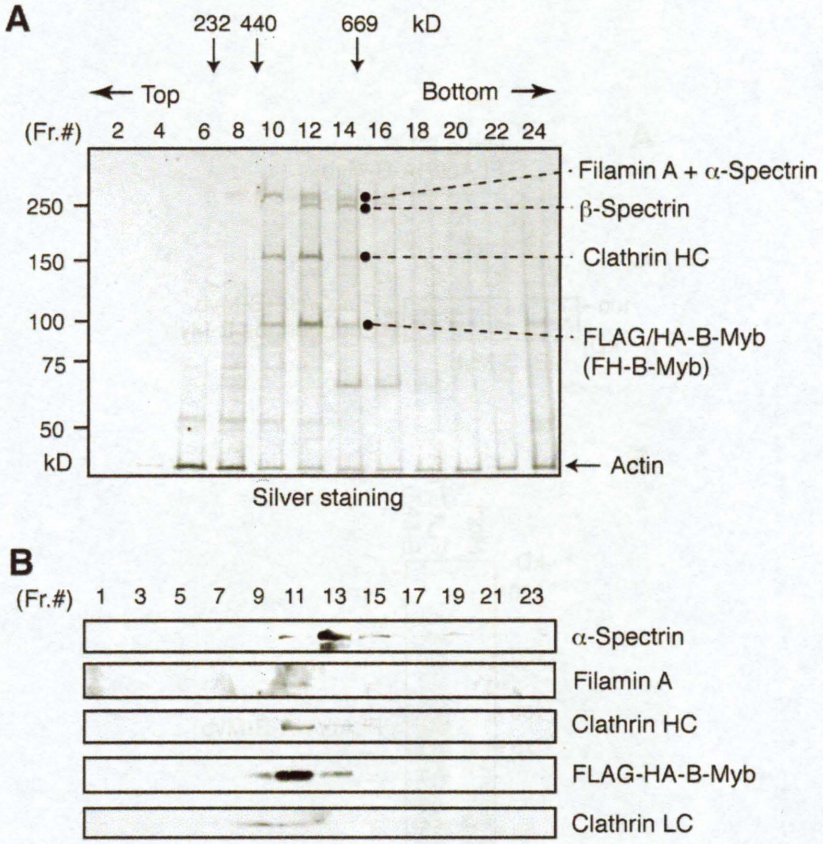
A
232 440
669
kD
Top
Bottom
(Fr.#) 2 4 6 8 10 12 14 16 18 20 22 24
250
150
100
75
50
kD
Filamin A + α-Spectrin
β-Spectrin
Clathrin HC
FLAG/HA-B-Myb
(FH-B-Myb)
Actin
Silver staining
B
(Fr.#) 1 3 5 7 9 11 13 15 17 19 21 23
α-Spectrin
Filamin A
Clathrin HC
FLAG-HA-B-Myb
Clathrin LC

Fig. 2.

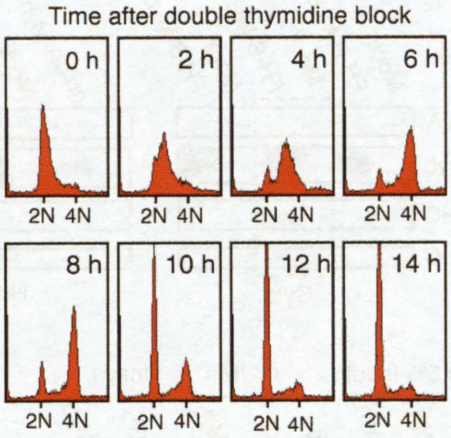
Time after double thymidine block
0 h
2 h
4 h
6 h
8 h
10 h
12 h
14 h
2N 4N

Fig. 3.

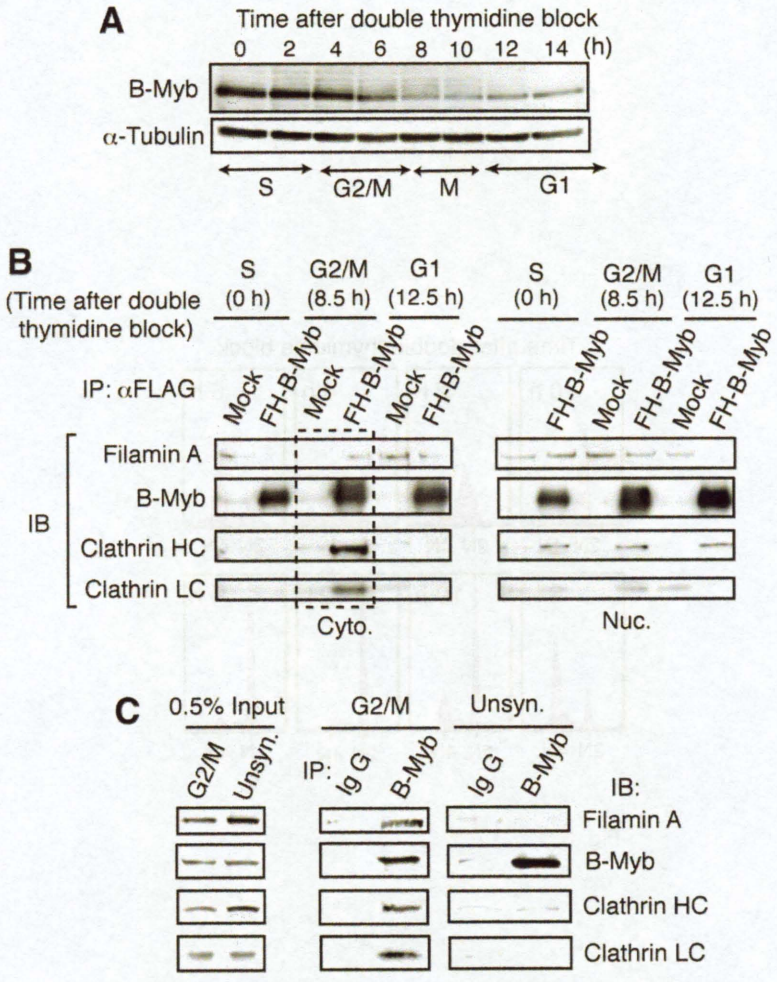
A
Time after double thymidine block
0 2 4 6 8 10 12 14 (h)
B-Myb
α-Tubulin
S
G2/M
M
G1
B
(Time after double thymidine block)
S (0 h)
G2/M (8.5 h)
G1 (12.5 h)
S (0 h)
G2/M (8.5 h)
G1 (12.5 h)
IP: αFLAG
Mock
FH-B-Myb
IB
Filamin A
B-Myb
Clathrin HC
Clathrin LC
Cyto.
Nuc.
C
0.5% Input
G2/M
Unsyn.
IP:
Ig G
B-Myb
IB:
Filamin A
B-Myb
Clathrin HC
Clathrin LC

Fig. 4.

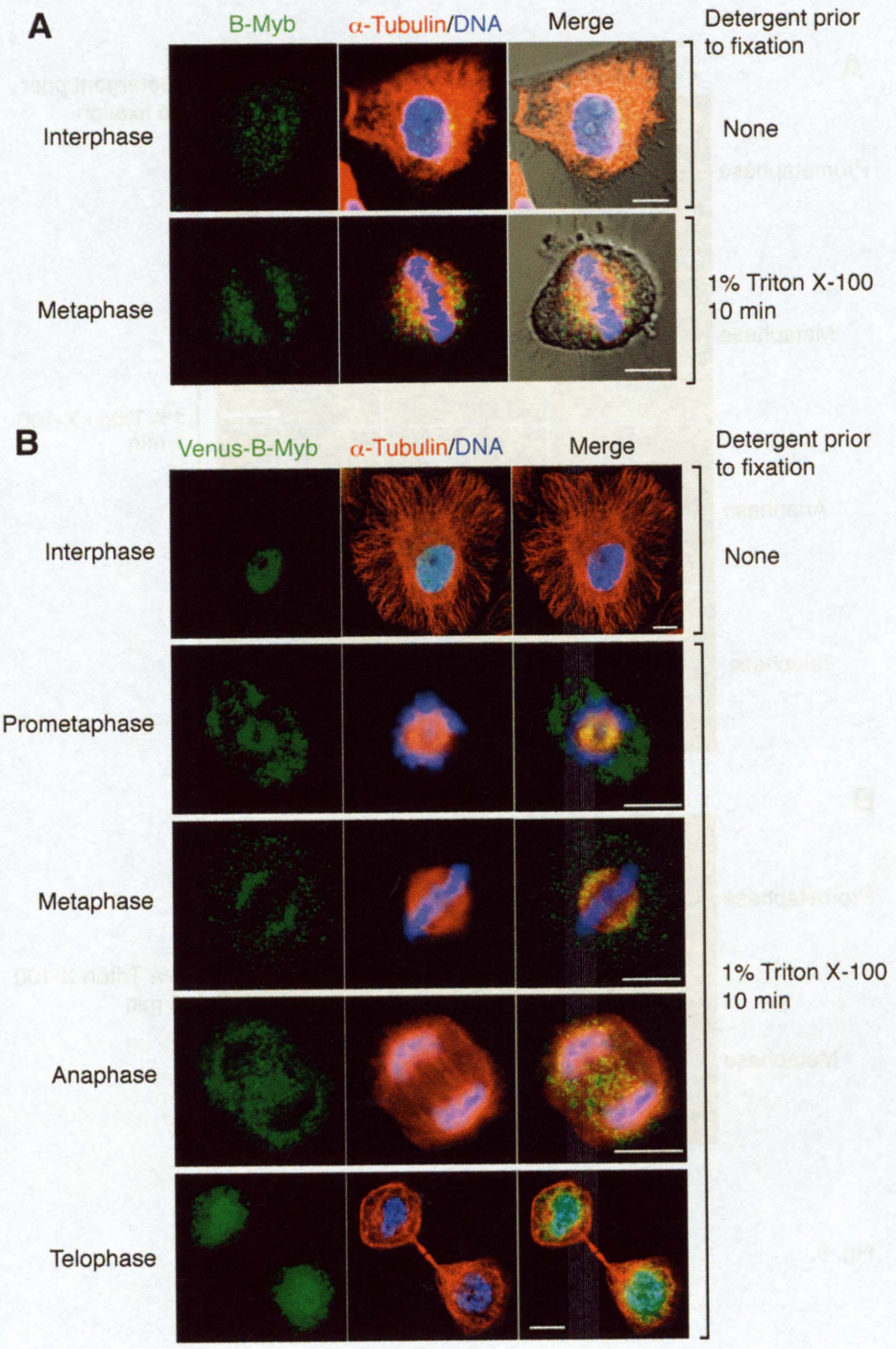
A
B-Myb
α-Tubulin/DNA
Merge
Detergent prior to fixation
Interphase
None
Metaphase
1% Triton X-100 10 min
B
Venus-B-Myb
α-Tubulin/DNA
Merge
Detergent prior to fixation
Interphase
None
Prometaphase
Metaphase
1% Triton X-100 10 min
Anaphase
Telophase

Fig. 5.

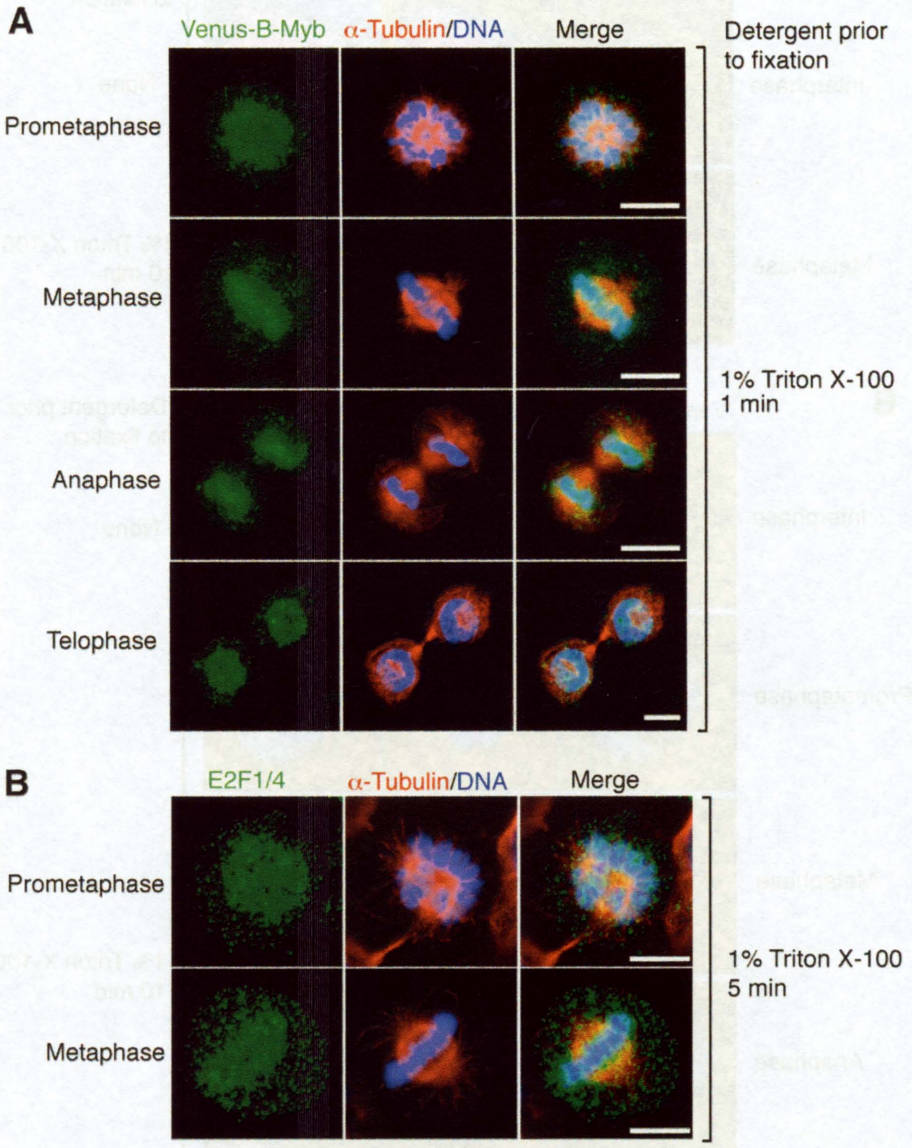
A
Venus-B-Myb
α-Tubulin/DNA
Merge
Detergent prior to fixation
Prometaphase
Metaphase
Anaphase
Telophase
1% Triton X-100
1 min
B
E2F1/4
α-Tubulin/DNA
Merge
Prometaphase
Metaphase
1% Triton X-100
5 min

Fig. 6.

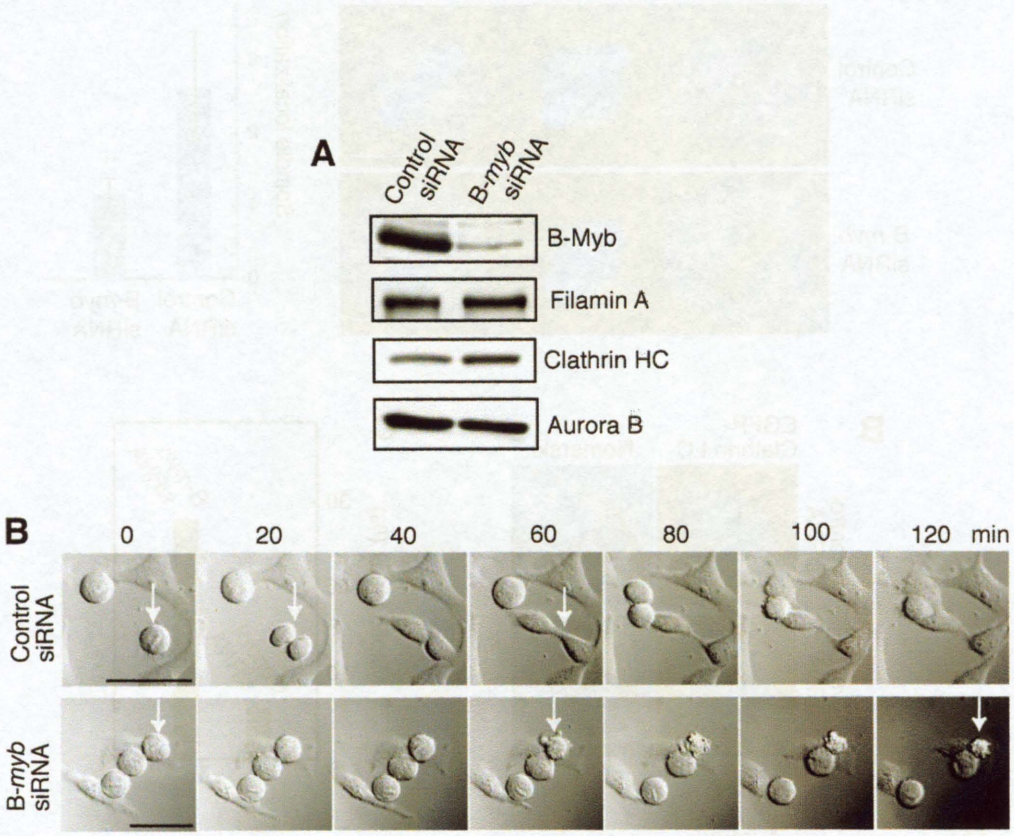
A
Control siRNA
B-myb siRNA
B-Myb
Filamin A
Clathrin HC
Aurora B
B
0
20
40
60
80
100
120 min
Control siRNA
B-myb siRNA

Fig. 7.

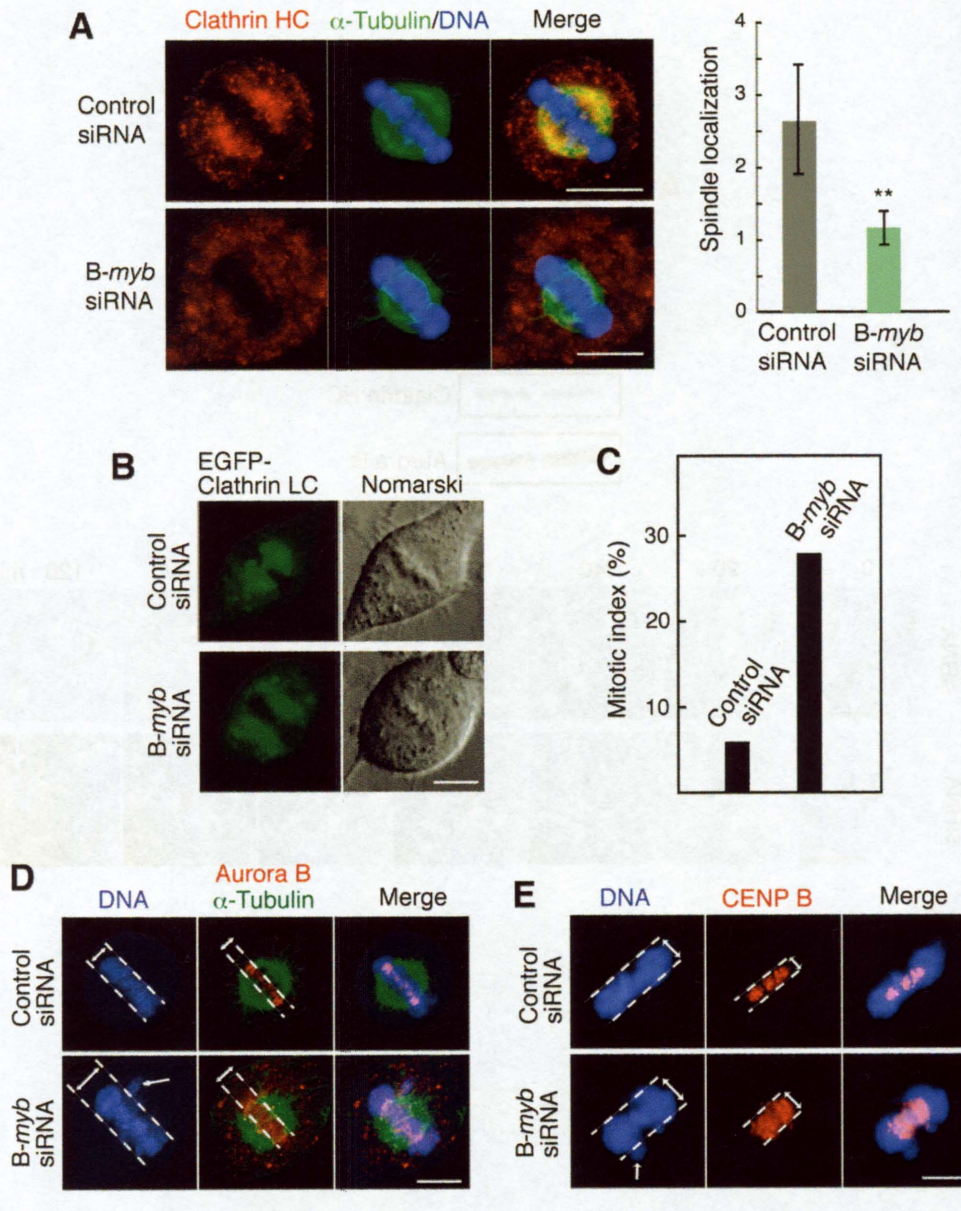
A
Clathrin HC
α-Tubulin/DNA
Merge
Control siRNA
B-myb siRNA
Spindle localization
4
3
2
1
0
**
Control siRNA
B-myb siRNA
B
EGFP-Clathrin LC
Nomarski
Control siRNA
B-myb siRNA
C
Mitotic index (%)
30
20
10
B-myb siRNA
Control siRNA
D
DNA
Aurora B
α-Tubulin
Merge
Control siRNA
B-myb siRNA
E
DNA
CENP B
Merge
Control siRNA
B-myb siRNA

Fig. 8.

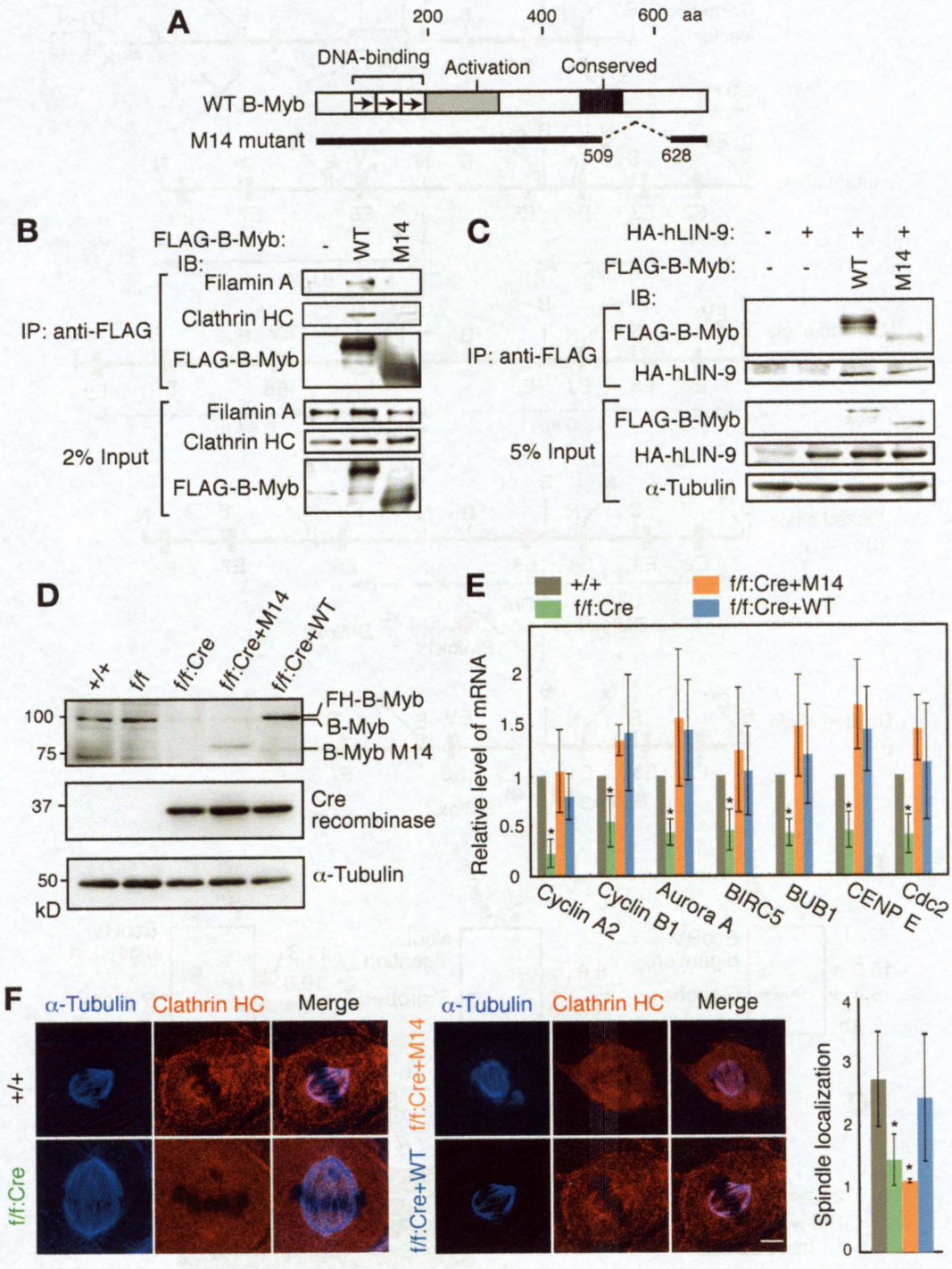
A
200
400
600 aa
DNA-binding
Activation
Conserved
WT B-Myb
M14 mutant
509
628
B
FLAG-B-Myb:
IB:
WT
M14
Filamin A
Clathrin HC
FLAG-B-Myb
IP: anti-FLAG
2% Input
C
HA-hLIN-9:
FLAG-B-Myb:
IB:
HA-hLIN-9
5% Input
α-Tubulin
D
+/+
f/f
f/f:Cre
f/f:Cre+M14
f/f:Cre+WT
FH-B-Myb
B-Myb
B-Myb M14
Cre recombinase
α-Tubulin
100
75
37
50
kD
E
+/+
f/f:Cre
f/f:Cre+M14
f/f:Cre+WT
Relative level of mRNA
Cyclin A2
Cyclin B1
Aurora A
BIRC5
BUB1
CENP E
Cdc2
F
α-Tubulin
Clathrin HC
Merge
f/f:Cre+M14
f/f:Cre+WT
Spindle localization

Fig. 9.

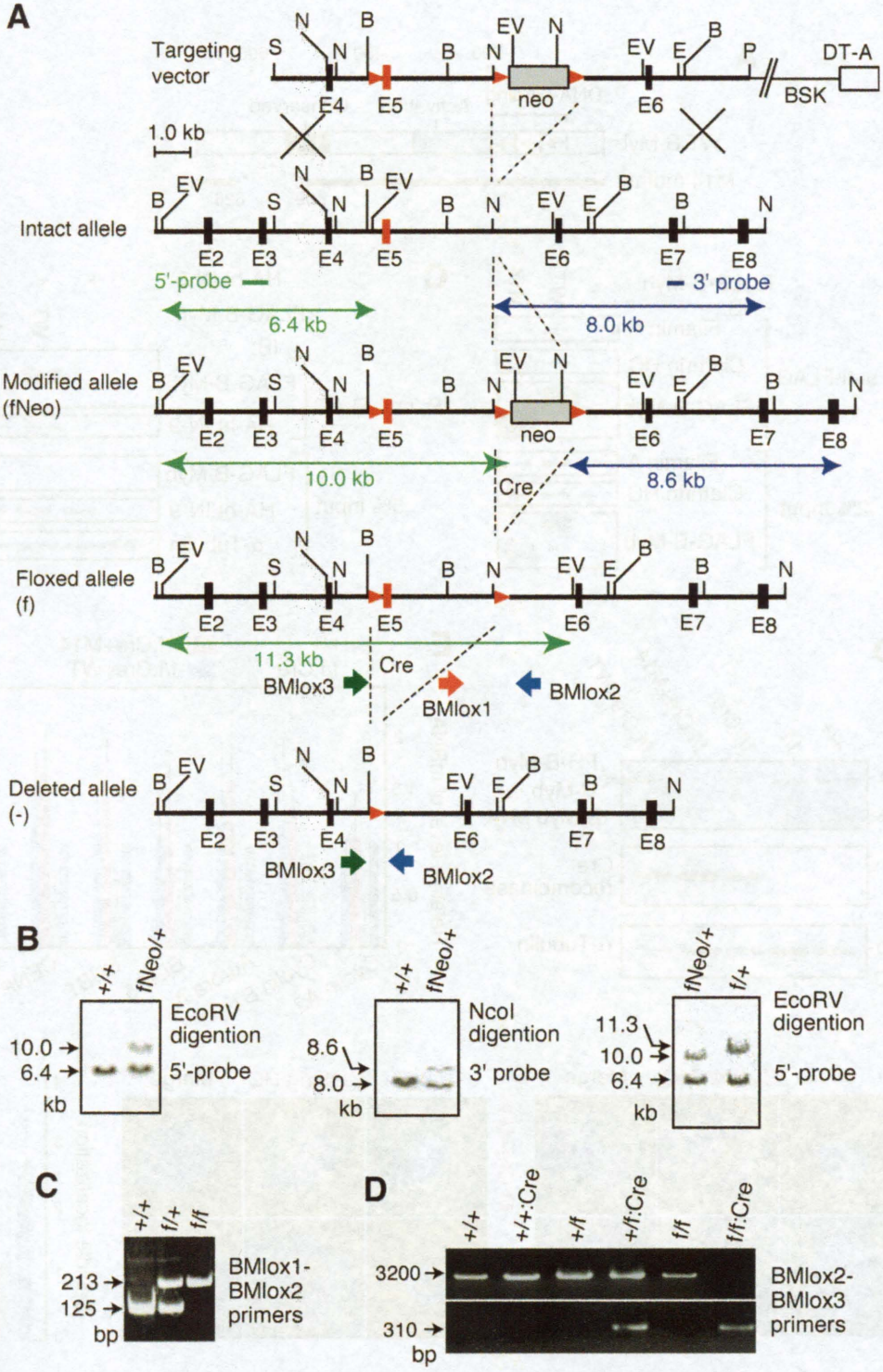
A
Targeting vector
DT-A
BSK
neo
1.0 kb
Intact allele
5'-probe
3' probe
6.4 kb
8.0 kb
Modified allele (fNeo)
10.0 kb
8.6 kb
Cre
Floxed allele (f)
11.3 kb
BMlox3
BMlox1
BMlox2
Deleted allele (-)
B
+/+
fNeo/+
EcoRV digention
5'-probe
10.0
6.4
kb
NcoI digention
3' probe
8.6
8.0
f/+
11.3
C
f/f
213
125
bp
BMlox1-BMlox2 primers
D
+/+:Cre
+/f
+/f:Cre
f/f:Cre
3200
310
BMlox2-BMlox3 primers

Fig. 10.

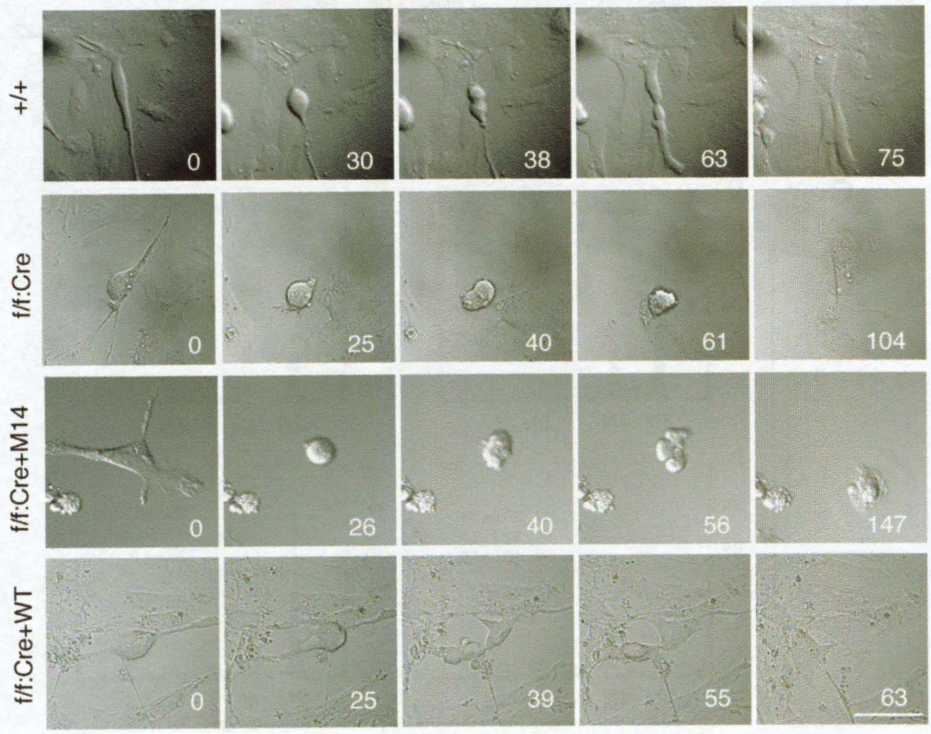
+/+
0
30
38
63
75
f/f:Cre
0
25
40
61
104
f/f:Cre+M14
0
26
40
56
147
f/f:Cre+WT
0
25
39
55
63

Fig. 11.

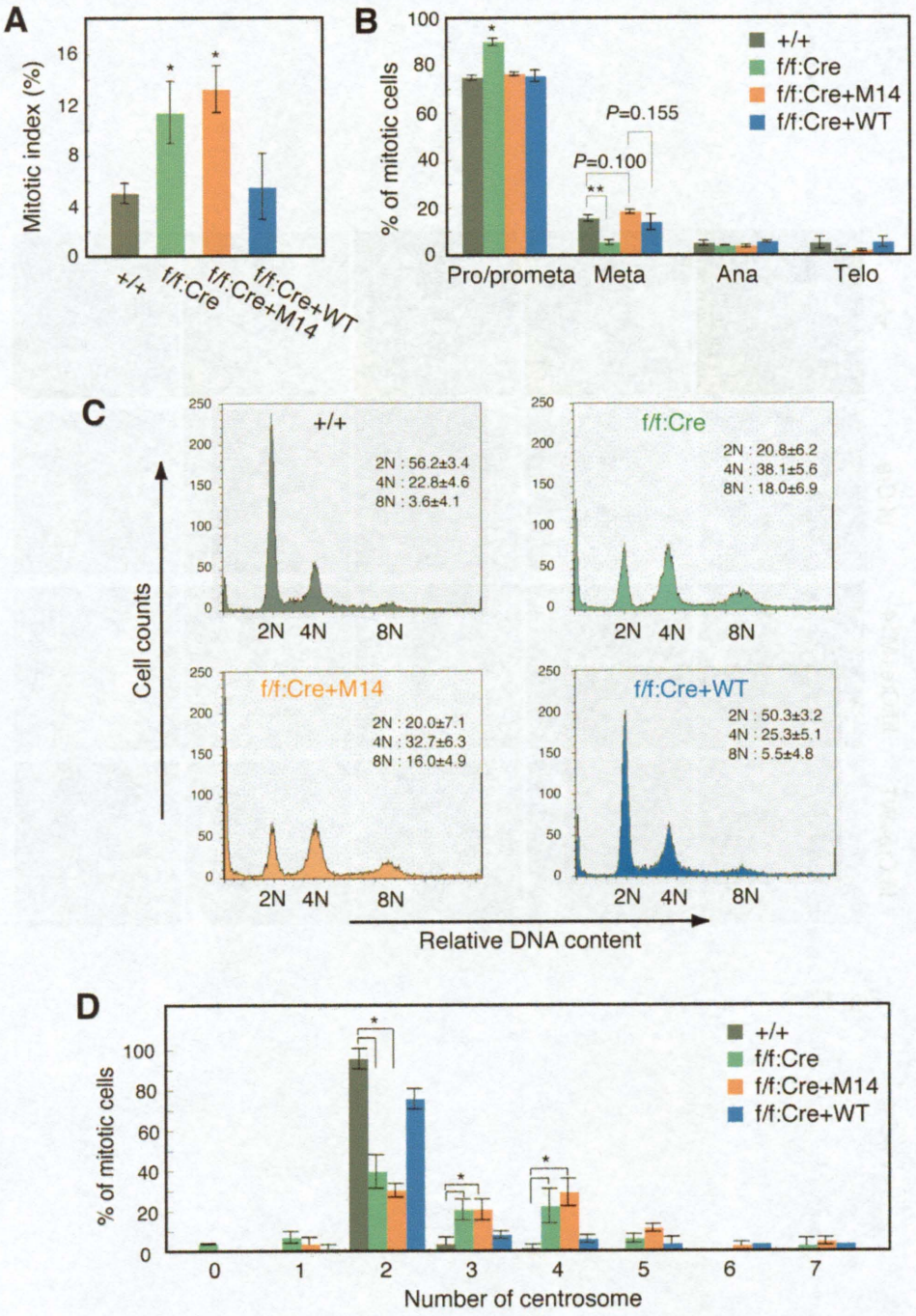
A
Mitotic index (%)
16
12
8
4
0
+/+
f/f:Cre
f/f:Cre+M14
f/f:Cre+WT
B
% of mitotic cells
100
80
60
40
20
0
+/+
f/f:Cre
f/f:Cre+M14
f/f:Cre+WT
P=0.155
P=0.100
Pro/prometa
Meta
Ana
Telo
C
Cell counts
+/+
2N : 56.2±3.4
4N : 22.8±4.6
8N : 3.6±4.1
f/f:Cre
2N : 20.8±6.2
4N : 38.1±5.6
8N : 18.0±6.9
f/f:Cre+M14
2N : 20.0±7.1
4N : 32.7±6.3
8N : 16.0±4.9
f/f:Cre+WT
2N : 50.3±3.2
4N : 25.3±5.1
8N : 5.5±4.8
2N 4N 8N
Relative DNA content
D
% of mitotic cells
+/+
f/f:Cre
f/f:Cre+M14
f/f:Cre+WT
0 1 2 3 4 5 6 7
Number of centrosome

Fig. 12.

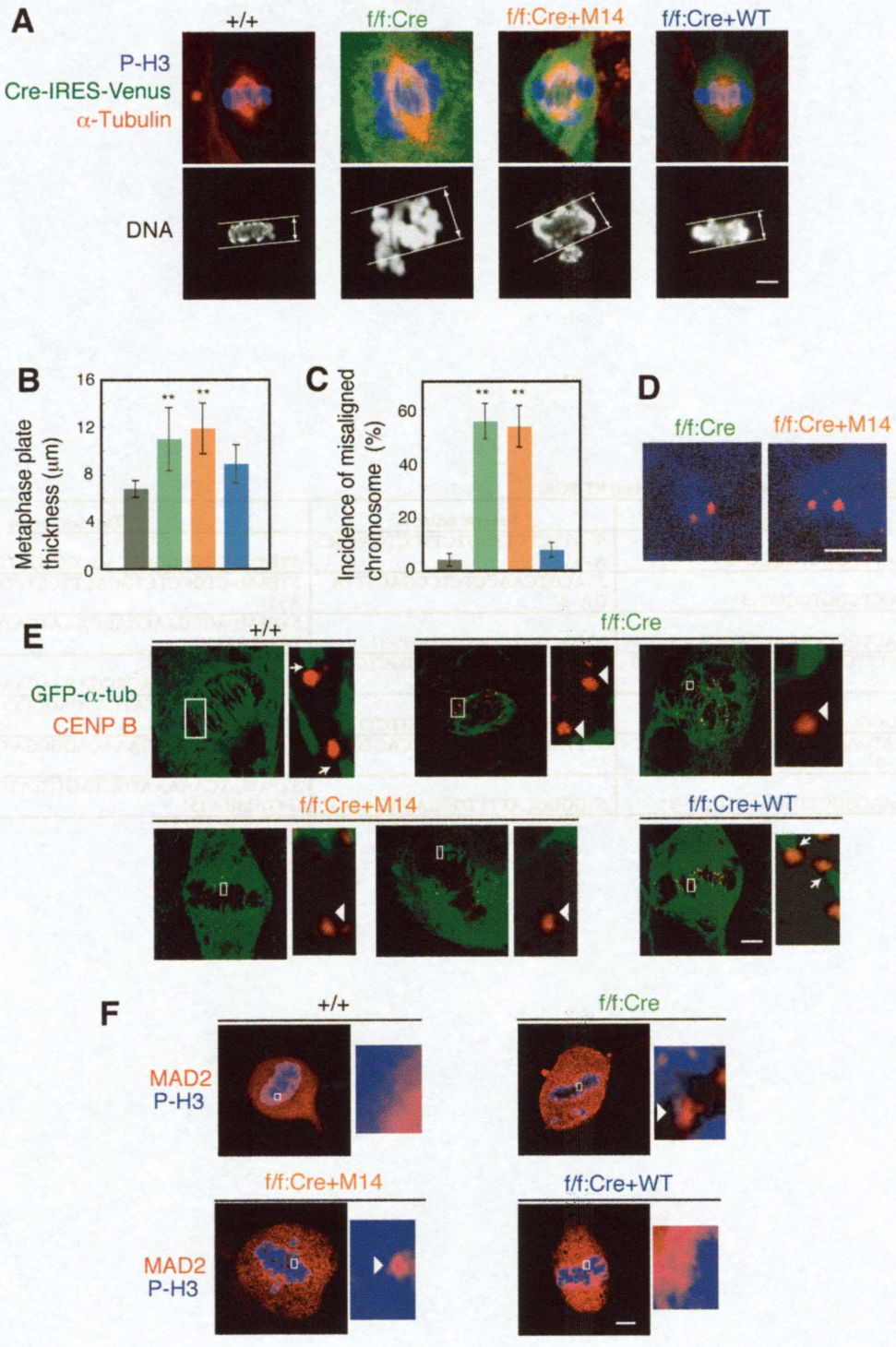
A
+/+
f/f:Cre
f/f:Cre+M14
f/f:Cre+WT
P-H3
Cre-IRES-Venus
α-Tubulin
DNA
B
Metaphase plate thickness (μm)
16
12
8
4
0
**
**
C
Incidence of misaligned chromosome (%)
60
40
20
0
**
**
D
f/f:Cre
f/f:Cre+M14
E
+/+
f/f:Cre
GFP-α-tub
CENP B
f/f:Cre+M14
f/f:Cre+WT
F
+/+
f/f:Cre
MAD2
P-H3
f/f:Cre+M14
f/f:Cre+WT
MAD2
P-H3

Fig. 13.

Table 1. Primers and probes used for real-time (TaqMan) RT-PCR.

	Forward primer	Reverse primer	TaqMan probe
Cyclin A2	5'-GGCATTCGGGTCGCG-3'	5'-ATTCTCTTGGTCTTCCTGATGCA-3'	5'(FAM)-TGCGGGCTCAGCCCTGCTCT-(TAMRA)3'
Cyclin B1	5'-CAGCCTGGGTCGCC-3'	5'-ACGTCAACCTCTCCGACTTTAGA-3'	5'(FAM)-CTGCCTCTGCACTTCCTCCGTAGAGC-(TAMRA)3'
Aurora A	5'-CCAACTGGCCACACTAGCAAA-3'	5'-CACGGTGGCCGTGGT-3'	5'(FAM)-AGCCAACCAGCAAATCATCTTAGGGAATCC-(TAMRA)3'
BIRC5	5'-GTTTTTTCTGCTTTAAGGAATTGG-3'	5'-GGGAGTGCTTTCTATGCTCCTCTA-3'	5'(FAM)-CTGGGAACCCGATGACAACCCG-(TAMRA)3'
Bub1	5'-GCCGCCGAGGCTCATC-3'	5'-GTGGCCTCACGGCTGTCTT-3'	5'(FAM)-ACTGTTCATCACCAGGCCCTCATCATAAAGA-(TAMRA)3'
CENP-E	5'-AAGATGAAGATAGACCTGTCATACACATC-3'	5'-TTAGCGTCAAGGGCCACTGT-3'	5'(FAM)-AGACCTGAAACAGGCGATGCGCA-(TAMRA)3'
Cdc2	5'-GAGAACGGCTTGGATTTGCT-3'	5'-GGGCCATTTTGCCAGAGAT-3'	5'(FAM)-TCAAAAATGCTAGTCTATGATCCTGCCAAACG-(TAMRA)3'

第二章

Ribosomal stress induces processing of Mybbp1a and its translocation from the nucleolus to the nucleoplasm

Tomohiro Yamauchi[1,2], Rebecca A. Keough[3], Thomas J. Gonda[4], and Shunsuke Ishii[1,2,*]

[1]Laboratory of Molecular Genetics, RIKEN Tsukuba Institute, 3-1-1 Koyadai, Tsukuba, Ibaraki 305-0074, Japan
[2]Graduate School of Comprehensive Human Sciences, University of Tsukuba, 1-1-1 Ten-noudai, Tsukuba, Ibaraki 305-8577, Japan
[3]School of Molecular and Biomedical Science, University of Adelaide, Adelaide, SA 5005, Australia.
[4]University of Queensland Diamantina Institute for Cancer, Immunology and Metabolic Medicine, Princess Alexandra Hospital, Ipswich Road, Brisbane, Qld 4102, Australia.

Running title: Processing of Mybbp1a

*Correspondence: E-mail: sishii@rtc.riken.jp

The total character count: 45,339

Abstract

Myb-binding protein 1a (Mybbp1a) was originally identified as a c-Myb-interacting protein, and also binds to various other transcription factors. The 160-kD Mybbp1a protein ($p160^{MBP}$) is ubiquitously expressed and is posttranslationally processed in some types of cells to generate an amino-terminal 67 kD fragment ($p67^{MBP}$). Despite its interaction with various transcription factors, Mybbp1a is localized predominantly, but not exclusively, in nucleoli. Here, we have purified the two Mybbp1a-containing complexes. The smaller complex contained $p67^{MBP}$ and $p140^{MBP}$ which lacked the C-terminal region of $p160^{MBP}$ containing the nucleolar localization sequences. The larger complex contained the intact $p160^{MBP}$ and various ribosomal subunits. Treatment of cells with actinomycin D, cisplatin, or UV, all of which inhibit ribosome biogenesis, induced processing of $p160^{MBP}$ into $p140^{MBP}$ and $p67^{MBP}$. Actinomycin D, cisplatin, and UV also induced a translocation of Mybbp1a from the nucleolus to the nucleoplasm. Both small and large Mybbp1a complexes contained nucleophosmin and nucleolin. In contrast, nucleostemin was detected only in the large complex, while the cell cycle-regulated protein EBP1 was only in the small complex. These results suggest that Mybbp1a may connect the ribosome biogenesis and the Myb-dependent transcription, which controls cell cycle progression and proliferation.

Introduction

Myb-binding protein 1a (Mybbp1a) was originally identified as an interacting partner of the c-*myb* proto-oncogene product (c-Myb) (Tavner *et al.*, 1998), which is critical for hemopoietic cell proliferation and differentiation (Mucenski *et al.*, 1991; Gewirtz and Calabretta, 1988). The 160-kD Mybbp1a protein ($p160^{MBP}$) is ubiquitously expressed and is posttranslationally processed in some types of cells to generate an N-terminal fragment of 67 kD ($p67^{MBP}$) (Tavner *et al.*, 1998). Both $p160^{MBP}$ and $p67^{MBP}$ bind to a leucine-rich region, which contains two $\phi XX\phi\phi$ (ϕ: hydrophobic amino acids) motifs, within the negative regulatory domain of c-Myb. The $\phi XX\phi\phi$ motif was initially demonstrated to be critical for interaction between nuclear hormone receptors and their coactivators (Heery *et al.*, 1997). In addition to Mybbp1a, multiple corepressors, including TIF1β and BS69, also bind to the leucine-rich region of c-Myb, and suppress c-Myb activity (Nomura *et al.*, 2004; Ladendorff *et al.*, 2001). Point mutations in this leucine-rich region enhance the c-Myb's capacity to activate transcription and to transform hematopoietic cells (Kanei-Ishii *et al.*, 1992). Although $p67^{MBP}$ reduces the *trans*-activating capacity of c-Myb by 80%, $p160^{MBP}$ does not affect c-Myb activity (Tavner *et al.*, 1998). It remains unknown what kinds of signals can induce the processing of $p160^{MBP}$ into $p67^{MBP}$, and why these two forms have different capacities to regulate c-Myb activity.

Mybbp1a also binds to a number of other transcription factors. Both $p160^{MBP}$ and $p67^{MBP}$ bind to the transcriptional coactivator PPARγ coactivator 1 α (PGC-1α) (Fan *et al.*, 2004), which is a key regulator of metabolic processes (Lin *et al.*, 2005). Binding of either form of Mybbp1a to PGC-1α represses the coactivator activity of PGC-1α, while the interaction between PGC-1α and Mybbp1a is disrupted by p38 MAPK phosphorylation of PGC-1α. $p160^{MBP}$ also directly binds to the transcription activation domain of the RelA/p65 subunit of NF-κB, and suppresses its *trans*-activating capacity by competing with p300 for binding to the transactivation domain of RelA/p65 (Owen *et al.*, 2007). $p160^{MBP}$ was recently identified as an component of the corepressor Ret-CoR complex, which mediates photoreceptor cell-specific nuclear receptor (PNR)-dependent repression (Takezawa *et al.*, 2007), although the role of $p160^{MBP}$ in this complex is unknown. These findings suggest that Mybbp1a functions as a corepressor in many situations, although Mybbp1a can also bind to the aryl hydrocarbon receptor (AhR), a basic helix–loop–helix/Per-Arnt-Sim (bHLH/PAS) transcription factor, to stimulate the transcriptional activation capacity of AhR (Jones *et al.*, 2002).

Endogenous Mybbp1a is predominantly localized in the nucleolus, although nucleoplasmic localization is also observed (Tavner *et al.,* 1998). Deletion analysis of $p160^{MBP}$ indicated that its carboxyl terminus, which contains several short basic amino acid repeat sequences, is responsible for both nuclear and nucleolar localization (Keough *et al.,* 2003). On the other hand, $p67^{MBP}$ is mainly localized in the cytoplasm when it is overexpressed by itself, suggesting that endogenous $p67^{MBP}$ is localized in the nuclei via interaction with another protein(s). Although the role of Mybbp1a in the nucleolus is unknown, Mybbp1a has some homology with Po15p of yeast *Saccharomyces cerevisiae,* which is required for rRNA production (Shimizu *et al.,* 2002).

Here, we report that the stress signals which inhibit ribosomal biosynthesis induce the processing of $p160^{MBP}$ into $p140^{MBP}$ and $p67^{MBP}$ and their translocation from the nucleolus to the nucleoplasm.

Results

Purification of the $p160^{MBP}$ complex

A HeLa S3 cell lines in which $p160^{MBP}$ tagged with both FLAG and HA is stably expressed, were generated by retroviral transduction. By Western blotting analysis we selected one of several clones that expressed FLAG/HA-$p160^{MBP}$ at the lowest level, and used this clone to purify the $p160^{MBP}$ complex, because its high level expression may induce imbalance between the components of the complex. Cells were disrupted in hypotonic buffer, and nuclei isolated. The $p160^{MBP}$ complex was purified from nuclear extracts by sequential immunoprecipitation with anti-FLAG and anti-HA antibodies, as described by Nakatani and Ogryzko (2003), followed by glycerol gradient centrifugation. Silver staining of SDS-PAGE gels of the purified proteins revealed two different-sized complexes (Fig. 14A). Mass spectrometric analysis indicated that the small complex contained $p140^{MBP}$, which lacks the C-terminal region of $p160^{MBP}$ as shown below, nucleolin (also called C23), $p67^{MBP}$, which is a an N-terminal fragment of Mybbp1a generated from $p160^{MBP}$, EBP1 (Erb3-binding protein), and nucleophosmin (also called B23). The large complex involved $p160^{MBP}$, $p140^{MBP}$, topoisomerase I, nucleolin, nucleostemin, nucleophosmin, histone H1x, and many ribosomal proteins. Nucleolin, nucleostemin, and nucleophosmin are nucleolar proteins, but are also localized in the nucleoplasm to some extent. Nucleolin is an acidic phosphoprotein and is involved in the transcriptional control of ribosomal RNA (rRNA) genes, in ribosome maturation and assembly, and in nucleocytoplasmic transportation of ribosomal components (Mongelard and Bouvet, 2006). Nucleostemin is a GTP-binding protein highly enriched in the stem cells and cancer cells (Tsai and McKay, 2002). Nucleophosmin is a phosphoprotein that plays roles in multiple steps of ribosome biogenesis, including ribosome assembly and transport, and is frequently overexpressed, mutated, and deleted in cancers (Grisendi *et al.,* 2006). EBP1 (also called PA2G4: proliferation-associated 2G4) was originally isolated using the antibody mAb2G4 which recognized the single-strand DNA-binding protein, and is highly expressed between G1 and mid-S phase (Radomski and Jost, 1995).

Western blotting using the mixture of antibodies, which were raised against the N- and C-terminal regions of $p160^{MBP}$ (Tavner *et al.,* 1998), indicated that the two complexes contained three different species of $p160^{MBP}$, which were also detected by silver staining of the gel, and that the smallest species ($p140^{MBP}$) was dominant in the small complex, while the largest species, which is likely to be an intact $p160^{MBP}$, was predominant in the large complex (Fig. 14B). Western blotting using specific antibodies confirmed the results of mass spectrometric analysis. Nucleolin and nucleophosmin were detected in both complexes. On the other hand, $p67^{MBP}$ and EBP1 were found only in the small complex, while nucleostemin and histone H1x were detected only in the large complex. We also confirmed complex formation by these proteins using co-immunoprecipitation. Nuclear extracts from HeLa cells expressing FLAG/HA-$p160^{MBP}$ were precipitated with anti-FLAG antibody, and the immunocomplexes were subjected to western blotting with specific antibodies. $p160^{MBP}$, $p140^{MBP}$, $p67^{MBP}$, nucleolin, nucleostemin, EBP1, nucleophosmin, and histone H1x were detected in the immunocomplexes (Fig. 14C).

Both $p140^{MBP}$ and $p67^{MBP}$ were detected in the small Mybbp1a complex, while the large complex contained both $p160^{MBP}$ and small amount of $p140^{MBP}$. These results raised the possibility that Mybbbp1a may form a dimer or an oligomer. To examine this, we investigated whether the $p160^{MBP}$ proteins intermolecularly interact each other using the GST-pull-down assays. *In vitro*-translated $p160^{MBP}$ bound to the GST fusion proteins containing $p67^{MBP}$ or the C-terminal 299-amino acids fragment of $p160^{MBP}$, while it did not interact with the GST protein alone (Fig. 14D). These results suggest that the Mybbp1a molecules can form a dimer or an oligomer.

Generation of $p140^{MBP}$ by removal of the C-terminal basic region of $p160^{MBP}$

The difference in the molecular weight between $p160^{MBP}$ and p $p140^{MBP}$ was about 20-40 kD, which was not likely due to modification such as phosphorylation. We examined the peptides generated from $p140^{MBP}$ which were identified by mass spectrometric analysis. The peptides detected covered the region between amino acids 6 and 1170 of $p160^{MBP}$ but no peptides were found that were derived from the C-terminal 174-amino acids of $p160^{MBP}$ (Fig. 15), suggesting that $p140^{MBP}$ is generated by removal of the C-terminal 170-amino acids. This C-terminal region contains a cluster of basic amino acids similar to a cluster in the N-terminal region of ARF that was reported to be responsible for nucleolar localization (Weber *et al.,* 1999). Furthermore, we (RAK and TJG) previously demonstrated that the C-terminal 193 amino acids of $p160^{MBP}$ was sufficient to confer nuclear

and nucleolar localization on β-galactosidase protein (Keough *et al.*, 2003). Together with these reports, our results suggest that the small complex containing p140^{MBP} and p67^{MBP} is generated by processing and may translocate from the nucleolus to the nucleoplasm.

Ribosomal stress induces the processing of p160^{MBP} to p140^{MBP} and p67^{MBP}

A recent report on mass-spectrometric analysis of nucleolar proteins (Andersen *et al.*, 2005) indicated that Mybbp1a is one such protein that is depleted from the nucleolus by treatment of cells with actinomycin D (ActD), which selectively inhibits rRNA gene transcription by low doses (Sollner-Webb and Tower, 1986; Scheer and Weisenberger, 1994). Very recently, Mybbp1a was shown to translocate from the nucleolus to the nucleoplasm by ActD treatment (Diaz et al., 2007). These results suggested to us the possibility that ActD treatment induces the processing of p160^{MBP} to p140^{MBP} and p67^{MBP}, and subsequent translocation of the small complex containing p140^{MBP} and p67^{MBP} from the nucleolus to the nucleoplasm. To examine this, we treated HeLa cells expressing FLAG/HA-p160^{MBP} with ActD, and prepared cell lysates at 12 h after ActD addition, which were then used for immunoprecipitation with anti-FLAG antibody followed by Western blotting with anti-Mybbp1a antibody. ActD treatment reduced the levels of p160^{MBP} by about 50%, and increased the levels of p140^{MBP} and p67^{MBP} (Fig. 16A), suggesting that ActD treatment induces the processing of p160^{MBP} to p140^{MBP} and p67^{MBP}.

Since ActD selectively inhibits the transcription of rRNA genes by low doses (Sollner-Webb and Tower, 1986; Scheer and Weisenberger, 1994), we attempted to examine whether other stresses or drugs that inhibit rRNA gene transcription also induced the processing of p160^{MBP} to p140^{MBP} and p67^{MBP}. Cisplatin, an anti-cancer drug, is known to inhibit the transcription of rRNA genes (Treiber *et al.*, 1994; Jordan and Carmo-Fonseca, 1998), and UV light irradiation was also reported to disrupt nucleoli (Zatsepina *et al.*, 1989). Treatment of HeLa cells expressing FLAG/HA-p160^{MBP} with cisplatin or UV irradiation also reduced the levels of p160^{MBP} by about 50%, and increased the levels of p140^{MBP} and p67^{MBP} (Fig. 16A), suggesting that inhibition of rRNA gene transcription induces the processing of p160^{MBP} to p140^{MBP} and p67^{MBP}.

ActD induces the translocation of the p67^{MBP}/p140^{MBP} complex from the nucleolus to the nucleoplasm

To examine whether ActD induces a translocation of p140^{MBP} and p67^{MBP} from the nucleolus to the nucleoplasm, HeLa cells expressing FLAG/HA-p160^{MBP} were treated with ActD, and the subcellular localization of FLAG/HA-Mybbp1a was analyzed. The FLAG/HA-Mybbp1a signals detected with the anti-FLAG antibody were predominantly in the nucleolus in the ActD-untreated cells (Fig. 16B). When cells were treated with ActD, significant amounts of Mybbp1a signals were detected in the nucleoplasm. The degree of increase in the levels of nucleoplasmic FLAG/HA-Mybbp1a by ActD treatment appears to be consistent with the degree of processing of p160^{MBP} to p140^{MBP} and p67^{MBP} shown in Figure 3A.

To confirm the translocation of Mybbp1a, we utilized time-lapse microscopic analysis. For this purpose we generated HeLa cells expressing a fusion of Venus, a GFP derivative (Nagai *et al.*, 2002) with p160^{MBP} (Venus-p160^{MBP}) (Fig. 17A). Time-lapse analysis of the subcellular localization of Venus-p160^{MBP} indicated that significant amounts of the Venus-Mybbp1a signal translocated from the nucleolus to the nucleoplasm from 30 min after ActD addition and reached plateau at about 2h (Fig. 17B). When ActD was washed out, Venus-Mybbp1 in the nucleoplasm was not re-translocated to the nucleoli at least during 6 h after ActD removal (Fig. 17C), although nucleophosmin re-translocated to the nucleoli within 6 h after ActD removal (data not shown). These results suggest that translocation of Mybbp1a to the nucleoplasm from the nucleoli is irreversible.

After ActD treatment of HeLa cells, nucleophosmin and nucleolin, which were involved in both small and large complexes, were also translocated from the nucleolus (Fig. 18A and 18B). On the other hand, the subcellular localization of nucleostemin, which was detected only in the large complex, was not so affected by ActD (Fig. 18A). These observations are consistent with the notion that ActD treatment generates the small complex containing p140^{MBP} and p67MBP, which was then translocated from the nucleolus to the nucleoplasm. EBP1, which was found only in the small complex, was mainly localized in dot-like structures in the nucleoplasm in ActD-untreated cells, while ActD treatment appeared to stimulate its translocation into the nucleolus (Fig. 18B). These results suggest that the subcellulat localization of these proteins is regulated by multiple mechanisms, not simply by interacting with Mybbp1a.

Ribosomal stress induces a translocation of endogenous Mybbp1a complex from the nucleolus to the nucleoplasm in NIH3T3 cells

To examine whether ActD induces a translocation of endogenous Mybbp1a from the nucleolus to the nucleoplasm, NIH3T3 cells were treated with ActD, and the subcellular localization of endogenous Mybbp1a was analyzed. The signals detected with the antibody raised against the N-terminal region of p160^{MBP}, which include p160^{MBP}, p140^{MBP}, and p67^{MBP}, were predominantly in the nucleolus in the ActD-untreated cells (Fig. 19). When cells were treated with ActD, significant amounts of Mybbp1a signals were detected in the nucleoplasm. After ActD treatment, nucleophosmin, which was involved in both small and large complexes, were also translocated from the nucleolus to some extent. Treatment of NIH3T3 cells with cisplatin or UV induced a translocation of Mybbp1a signals from the nucleolus into the nucleoplasm (Fig. 19). Nucleophosmin was also similarly translocated from the nucleolus to the nucleoplasm by treatment with cisplatin or UV irradiation.

CTCF is associated with the Mybbp1a complexes

Nucleophosmin was detected in both small and large Mybbp1a complexes (Fig. 14A, B). Nucleophosmin was recently shown to be a component of a complex containing CTCF (CCCTC-binding factor), which binds to insulator elements and blocks enhancers of one gene from activating a promoter on another nearby gene (Yusufzai *et al.,* 2004). The CTCF complex also contained topoisomerase II, histone H1x, and several 40S ribosomal subunit proteins, while the large Mybbp1a complex contained topoisomerase, histone H1x, and many ribosomal subunits. This similarity raised the possibility that the Mybbp1a complexes may interact with CTCF, which we examined using co-immunoprecipitation. Cell lysates from HeLa cells expressing FLAG/HA-p160^{MBP} were immunoprecipitated with anti-FLAG antibody, and the immunocomplexes were subjected to Western blotting with anti-CTCF antibody. Figure 20A shows that CTCF was co-immunoprecipitated with FLAG/HA-p160^{MBP} and furthermore, that poly(ADP-ribose) polymerase (PARP), which has been detected in the CTCF complex (Yusufzai *et al.,* 2004), was also co-immunoprecipitated with FLAG/HA-p160^{MBP}.

To further confirm inclusion of CTCF in Mybbp1a complexes, we analyzed glycerol gradient fractions separating the large and small complexes by Western blotting using anti-CTCF antibodies. The results indicated that both the small and large Mybbp1a complexes contained CTCF (Fig. 20B), suggesting that CTCF is associated with Mybbp1a both in the nucleoplasm and in the nucleoli. Subcellular localization analysis using NIH3T3 cells further indicated that endogenous CTCF, histone H1, and PARP proteins were predominantly localized in the nucleoplasm (Fig. 20C), although small amounts of CTCF may also exist in the nucleoli as reported previously (Torrano *et al.,* 2006). Furthermore, CTCF, histone H1, and PARP proteins did not translocate into the nucleolus from the nucleoplasm after ActD treatment (Fig. 20C). These results suggest that the CTCF complex is associated with both the small and large Mybbp1a complexes in the nucleoplasm and the nucleoli, although translocation of CTCF itself is not affetced by ActD.

Discussion

Analysis of the two Mybbp1a complexes has suggested that the small Mybbp1a complex is generated by processing of full-length p160^{MBP} to p140^{MBP} and p67 ^{MBP}. p140^{MBP} lacks the C-terminal 20-kD fragment of p160^{MBP} which contains the nucleolar localization signals. ActD, which inhibits the transcription of rRNA genes, induced the processing of full-length p160^{MBP} to p140^{MBP} and p67 ^{MBP} and concomitantly, translocation of some of the Mybbp1a immunofluorescence from the nucleolus to the nucleoplasm. This translocation may be the consequence of the loss of nucleolar localization signal sequence from Mybbp1a.

The large Mybbp1a complex contained nucleolin, nucleostemin, nucleophosmin, and many ribosomal subunit proteins. Nucleolin and nucleophosmin are known to stimulate ribosome biogenesis by participating in multiple steps, including the transcription of rRNA genes, ribosome maturation, assembly, and ribosome transport (Mongelard and Bouvet, 2006; Grisendi *et al.,* 2006). The fact that nucleostemin, a GTP-binding protein, is enriched in the actively proliferating cells, such as stem cells and cancer cells (Tsai and McKay, 2002), is also consistent with its possible role in ribosome biogenesis. Thus, the role of these three nucleolar proteins and the involvement of many ribosomal subunits strongly suggest that the large Mybbp1a complex stimulates ribosome biogenesis. Consistent with this, Mybbp1a has a significant homology with the yeast protein Pol5p, which were shown to bind to the rRNA gene promoter (Shimizu *et al.,* 2002; Nadeem *et al.,* 2006). Although Pol5p shows some similarity with DNA polymerases, subsequent computational analysis of the sequence indicated that Pol5p is not a DNA polymerase (Yang *et al.,* 2003).

The small Mybbp1a complex contained nucleolin and nucleophosmin in addition to p140^{MBP} and p67^{MBP}. Since both p140^{MBP} and p67^{MBP} lack the nucleolar localization signals in the C-terminal region of p160^{MBP}, this complex is likely to be translocated into the nucleoplasm immediately after processing where it can interact with various transcription factors. Previously, we demonstrated that p67^{MBP}, but not p160^{MBP}, inhibited the c-Myb-dependent *trans*-activation (Tavner *et al.,* 1998). This may be because overexpression of p160^{MBP} does not lead to an increase in the amounts of the small Mybbp1a complex in the nucleoplasm. Although the mechanism by which the small Mybbp1a complex inhibits the c-Myb activity remains unknown, it was reported that nucleolin directly binds to the DNA-binding domain of c-Myb and inhibits the c-Myb-dependent *trans*-activation (Ying *et al.,* 2000).

The Mybbp1a complexes and the CTCF complex share some components: nucleophosmin, topoisomerase, some ribosomal subunits, and histone H1x. Furthermore, CTCF was co-immunoprecipitated with Mybbp1a, and detected in the purified Mybbp1a complexes. Yusufzai *et al.* (2004) previously reported the evidence that the insulator, which binds to CTCF, is drawn to the nucleolar surface by its strong interaction with nucleophosmin, and proposed that the CTCF/nucleophosmin complex creates separate loop domain structures to prevent the passage of a processive activating complex from the distal enhancer to the promoter. Therefore, the small Mybbp1a complex may also suppress transcription from Myb binding site-containing promoters by recruiting Myb bound to such sites to the nucleolar surface. We have detected CTCF not only in the small Mybbp1a complex but also in the large Mybbp1a complex, which appears to be in the nucleolus. Recently, it was reported that CTCF is localized in the nucleoli of differentiated cells and nucleolar localization of CTCF is associated

with growth arrest and inhibition of rRNA gene transcription (Torrano *et al.*, 2006). Therefore, CTCF may inhibit ribosome biogenesis by interacting with the Mybbp1a large complex in the nucleoli.

Since transcription of rRNA genes and the biosynthesis of ribosomes in the nucleolus are the major and limiting metabolic activities, the rate of ribosome biogenesis is tightly linked to cellular proliferation. Furthermore, recent data suggest that the nucleolus also plays an important role in cell-cycle regulation and senescence (Visintin & Amon, 2000; Guarente, 1997; Sherr & Weber, 2000). ActD, cisplatin, and UV irradiation, all of which inhibit ribosome biogenesis, induced the translocation of the small Mybbp1a complex from the nucleolus to the nucleoplasm. We suggest that the nucleolar large Mybbp1a complex acts to stimulate the ribosome biogenesis, while the nucleoplasmic small Mybbp1a complex may bind to c-Myb, leading to suppression of c-Myb-dependent transcription. c-Myb positively regulates cell cycle progression by activating several cell-cycle regulating genes, such as c-*myc* and *cyclin B1* (Nakagoshi *et al.*, 1992; Nakata *et al.*, 2007). c-Myb also suppresses apoptosis by inducing some anti-apoptotic genes, such as *bcl-2* (Frampton *et al.* 1996; Taylor *et al.* 1996). Thus, translocation of Mybbp1a from the nucleolus to the nucleoplasm upon ribosome stress may play an important role to block the cell cycle progression and to induce apoptosis by suppressing these c-Myb target genes. Mybbp1a also binds to the RelA/p65 subunit of NF-κB, and PGC-1α. Like c-Myb, NF-κB positively regulates cellular proliferation (Viatour *et al.*, 2005), while PGC-1α is a key regulator for energy production in mitochondria (Lin *et al.*, 2005). Therefore, the inhibition of NF-κB and PGC-1α by Mybbp1a may also contribute to suppression of cellular proliferation and energy production upon ribosome stress. Thus, Mybbp1a could be a key regulator that connects ribosome biogenesis and transcription to control cell cycle progression, proliferation, and energy production, as illustrated in Figure 21.

Interestingly, EBP1, which was detected in the small Mybbp1a complex, is highly expressed between G1 and mid-S phase (Radomski and Jost, 1995). This suggests that the amounts of small Mybbp1a complex could vary depending on the cell cycle, with a high level at the G1/S phase boundary. c-Myb was reported to be needed for G1/S transition in normal human T-lymphocytes (Gewirtz *et al.*, 1989), and is thought to regulate G1/S transition by inducing some target genes, including c-*myc* (Nakagoshi *et al.*, 1992). Therefore, the Mybbp1a complex may also play a role in suppressing excess c-Myb activity at G1/S phase.

Experimental Procedures

Complex purification

To generate a retroviral vector expressing FLAG- and HA-tagged p160^{MBP}, the mouse *p160^{MBP}* cDNA was cloned into the pOZ-FH-N vector (Nakatani and Ogryzko, 2003). The vector was transfected into the amphotropic packaging Phoenix A cell line and medium containing the amphotropic virus was prepared. HeLa S3 cells were transduced with a recombinant retrovirus expressing a bicistronic mRNA encoding FLAG/HA-p160^{MBP} linked to the IL-2 receptor subunit, and the transduced subpopulation was purified by repeated cycles of affinity cell sorting. After sorting, cells were plated onto 96-well plate and single cell clones were isolated. Cells were disrupted in hypotonic buffer (10 mM HEPES, pH 7.9, 1.5 mM $MgCl_2$, 10 mM KCl, 0.5 mM DTT), and the nuclear pellet was collected by centrifugation at 25,000 g for 20 min. The pellet was extracted with buffer C (20 mM HEPES, pH 7.9, 25% glycerol, 420 mM NaCl, 1.5 mM $MgCl_2$, 0.2 mM EDTA, 0.5 mM PMSF, 0.5 mM DTT) for 30 min at 4 °C and lysates were collected by centrifugation at 25,000 g for 30 min. The p160 complex was immunoprecipitated from nuclear extracts prepared from HeLa cells expressing p160 by incubating with M2 anti-FLAG agarose (Sigma) for 4 h with rotation. After an extensive wash with wash buffer (20 mM Tris-HCl, pH 8.0, 0.1 M KCl, 5 mM $MgCl_2$, 10% glycerol, 1 mM PMSF, 0.1% Tween 20, 10 mM β-mercaptoethanol), the bound proteins were eluted from the M2 agarose by incubation for 30 min with 0.2 mg/ml FLAG peptide (Sigma) in the same buffer. The eluates were further purified by immunoprecipitation with protein G-Sepharose (Amersham) conjugated to the anti-HA 12CA5 antibody. The bound proteins were eluted from the matrix by incubating for 60 min with 0.5 mg/ml HA peptide in wash buffer. The purified proteins was separated by 4–20% gradient SDS polyacrylamide gel electrophoresis (SDS–PAGE) and silver stained. For glycerol gradient sedimentation, 200 μl of FLAG antibody-immunoprecipitated material was loaded onto a 4.2 ml 10%–40% glycerol gradient in wash buffer. After centrifugation at 55,000 rpm for 1 h (Beckman, SW55Ti), 200 μl fractions were collected from the top of the gradient and resolved by 4-20% gradient SDS-PAGE and silver stained. The p160 complex fractions were TCA precipitated, resolved by 4-20% gradient SDS-PAGE and stained with Coomassie blue. Protein bands were excised and analyzed by a Biflex III MALDI-TOF mass spectrometer (Bruker Daltonics).

Culture and transfection of cells

HeLa cells and NIH3T3 cells were cultured in MEM or DMEM supplemented with 10% calf serum (CS), 100 U/ml penicillin G sodium and 100 μg/ml streptomycin sulfate at 37 °C and in 5 % CO_2.

Co-immunoprecipitation.

HeLa S3 cells expressing FLAG/HA-p160^{MBP} from a 200 mL culture were disrupted in hyptonic buffer (10 mM HEPES, pH 7.9, 1.5 mM $MgCl_2$, 10 mM KCl, 0.5 mM DTT), and the nuclear pellet was collected by

centrifugation at 15,000 g for 20 min. The pellet was extracted with buffer C (20 mM HEPES, pH 7.9, 25% glycerol, 420 mM NaCl, 1.5 mM $MgCl_2$, 0.2 mM EDTA, 0.5 mM PMSF, 0.5 mM DTT) for 30 min at 4 °C and lysates were collected by centrifugation at 15,000 g for 30 min. The Mybbp1a complex was immunoprecipitated from the extracts by incubating with M2 anti-FLAG agarose (Sigma) for 4 h with rotation. After five washes with wash buffer (20 mM Tris-HCl, pH 8.0, 0.1 M KCl, 5 mM $MgCl_2$, 10% glycerol, 1 mM PMSF, 0.1% Tween 20, 10 mM β-mercaptoethanol), the bound proteins were eluted from M2 agarose by incubation for 30 min with 0.2 mg/ml FLAG peptide (Sigma) in the same buffer. The immuno-complexes were analyzed by SDS-PAGE, followed by Western blotting using anti-Mybbp1a (Tavner *et al.*, 1998); anti-EBP1 (07-397, Upstate); anti-nucleophosmin (18-7288, Zymed); anti-C23 (nucleolin) (sc-8031, Santa Cruz Biotechnology) anti-nucleostemin (AF1638, R&D Systems); anti-CTCF (06-917, Upstate); anti-Histone H1 (05-457, Upstate); anti-PARP (SA-253, Biomol). Anti-Mybbp1a antibodies used a mixture of two polyclonal antibodies raised against the N-terminal 326 residues or C-terminal 298 residues of $p160^{MBP}$ (Tavner *et al.*, 1998).

GST pulldown assay.
GST pull-down assay was performed as described (Nomura *et al.*, 1999). The binding buffer used consisted of 20 mM HEPES, pH 7.9, 75 mM KCl, 0.05% NP-40, 1.25 mM $MgCl_2$, 0.1 mM EDTA, 1 mM DTT. GST fusion proteins bound to Glutathione-Sepharose 4B were mixed with ^{35}S-p160 translated *in vitro*, and the bound proteins were analyzed by SDS-PAGE, followed by autoradiography.

Generation of HeLa cells expressing Venus-$p160^{MBP}$
A retrovirus construct expressing a $p160^{MBP}$ fusion protein with Venus, a GFP derivative (Nagai *et al.*, 2002), was constructed using the pOZ-FH-N vector after removal of the FLAG-HA tag, and virus was prepared as described above. HeLa cells expressing Venus-$p160^{MBP}$ were selected as described above. To detect the Venus-$p160^{MBP}$ proteins, cell lysates were prepared using buffer C, and subjected to SDS-PAGE, followed by western blotting with anti-GFP (598, Medical Biological Laboratories).

Immunofluorescence microscopy
Cells were grown in 35 mm petri dishes, fixed with 4% paraformaldehyde in phosphate-buffered saline (PBS) for 20 min at room temperature. After incubation for 60 min with 3% skimmilk in PBS, cells were incubated for 1 h with the following primary antibodies: anti-Mybbp1a (rabbit polyclonal); anti-FLAG (M2, Sigma); anti-EBP1 (07-397, Upstate); anti-nucleophosmin (18-7288, Zymed); anti-C23 (nucleolin) (sc-8031, Santa Cruz Biotechnology) anti-nucleostemin (AF1638, R&D Systems). Anti-Mybbp1a antibody used here was raised against the N-terminal 326 residues of $p160^{MBP}$, and recognize $p160^{MBP}$, $p140^{MBP}$, and $p67^{MBP}$. The cells were washed, incubated with Alexa Fluor 488- or Cy3- or Rhodamine-conjugated anti-rabbit, anti-mouse, or anti-goat secondary antibodies (Molecular Probes or Chemicon). Chromatin was labeled with TOTO-3 iodide (Molecular Probes).

Confocal images were obtained using an LSM510 (Zeiss) laser scanning microscope. In order to minimize overlapping signals, images were obtained by sequential excitation at 488/543/633 nm, to detect Alexa Fluor 488, Cy3, and TOTO-3, respectively, and emission signals were detected at 505-530 nm for Alexa Fluor 488, >560 nm for Cy3, and >650 nm for TOTO-3 iodide. Images were processed using Photoshop software.

Time-lapse imaging
Cells were cultured in poly-D-lysine coated glass bottom 35 mm dishes (IWAKI). For observation of living cells, medium was replaced with fresh DMEM containing 20 mM HEPES (pH 7.4). Dishes were imaged at 37 °C using a Tempcontrol 37-2 chamber (Zeiss). Images were obtained using an LSM510 (Zeiss) laser scanning microscope. Images were captured at set time intervals for a period of at least 3 h. Images were processed using the Zeiss LSM image software.

Acknowledgements

We are grateful to Y. Nakatani for the pOZ-FH-N vector, and the staff of the Research Resources Center of the RIKEN Brain Science Institute for mass spectrometric analysis. This work was supported by Grants-in-aid for Scientific Research and by grants from the Genome Network project of the Ministry of Education, Culture, Sports, Science and Technology of Japan.

References

Andersen, J. S., Lam, Y. W., Leung, A. K., Ong, S. E., Lyon, C. E., Lamond, A. I. & Mann, M. (2005) Nucleolar proteome dynamics. *Nature* **433,** 77-83.

Diaz, V. M., Mori, S., Longobardi, E., Menendez, G., Ferrai, C., Keough, R. A., Bachi, A. & Blasi, F. (2007) p160 myb-binding-protein interacts with Prepl and inhibits its transcriptional activity. *Mol. Cell. Biol.* Sep

17; [Epub ahead of print]
Fan, M., Rhee, J, St-Pierre, J, Handschin, C., Puigserver, P., Lin, J, Jaeger, S., Erdjument-Bromage, H., Tempst, P. & Spiegelman, B. M. (2004) Suppression of mitochondrial respiration through recruitment of p160 myb binding protein to PGC-1 : modulation by p38 MAPK. *Genes Dev.* **18,** 278-289.
Frampton, J., Ramqvist, T. & Graf, T. (1996) v-Myb of E26 leukemia virus up-regulates bcl-2 and suppresses apoptosis in myeloid cells. *Genes Dev.* **10,** 2720-2731.
Gewirtz, A. M., Anfossi, G., Venturelli, D., Valpreda, S., Sims, R. & Calabretta, B. (1989) G1/S transition in normal human T-lymphocytes requires the nuclear protein encoded by c-*myb*. *Science* **245,** 180-183.
Gewirtz, A. M. & Calabretta, B. (1988) A c-*myb* antisense oligodeoxynucleotide inhibits normal human hematopoiesis in vitro. *Science* **242,** 1303-1306.
Grisendi, S., Mecucci, C., Falini, B. & Pandolfi, P. P.. (2006) Nucleophosmin and cancer. *Nature Rev. Cancer* **6,** 493-505.
Guarente, L. (1997) Link between aging and the nucleolus. *Genes Dev.* **11,** 2449-2455 .
Heery, D. M., Kalkhoven, E., Hoare, S. & Parker, M. G. (1997) A signature motif in transcriptional co-activators mediates binding to nuclear receptors. *Nature* **387,** 733-736
Jones, L. C., Okino, S. T., Gonda, T. J. & Whitlock, J. P. Jr. (2002) Myb-binding protein 1a augments AhR-dependent gene expression. *J. Biol. Chem.* **277,** 22515-22519.
Jordan, P. & Carmo-Fonseca, M. (1998) Cisplatin inhibits synthesis of ribosomal RNA in vivo. *Nucleic Acids Res.* **26,** 2831-2836.
Kanei-Ishii, C., MacMillan, E .M., Nomura, T., Sarai, A., Ramsay, R. G., Aimoto, S., Ishii, S. & Gonda, T. J. (1992) Transactivation and transformation by Myb are negatively regulated by a leucine-zipper structure. *Proc. Natl. Acad. Sci. USA* **89,** 3088-3092.
Keough, R. A., Macmillan, E. M., Lutwyche, J. K., Gardner, J. M., Tavner, F. J, Jans, D. A., Henderson, B. R. & Gonda, T. J. (2003) .Myb-binding protein 1a is a nucleocytoplasmic shuttling protein that utilizes CRM1-dependent and independent nuclear export pathways. *Exp. Cell Res.* **289,** 108-23.
Ladendorff, N. E., Wu, S. & Lipsick, J. S. (2001) BS69, an adenovirus E1A-associated protein, inhibits the transcriptional activity of c-Myb. *Oncogene* **20,** 125-132
Lin, J., Handschin, C. & Spiegelman, B. M. (2005) Metabolic control through the PGC-1 family of transcription coactivators. *Cell Metab.* **1,** 361-370.
Mongelard, F. & Bouvet, P. (2007) Nucleolin: a multiFACeTed protein. *Trends Cell Biol.* **17,** 80-86.
Mucenski, M. L., McLain, K., Kier, A. B., Swerdlow, S. H., Schreiner, C. M., Miller, T. A., Pietryga, D. W., Scott, W. J. Jr. & Potter, S. S. (1991) A functional c-*myb* gene is required for normal murine fetal hepatic hematopoiesis. *Cell* **65,** 677–689.
Nadeem, F. K., Blair, D., McInerny, C. J. (2006) Pol5p, a novel binding partner to Cdc10p in fission yeast involved in rRNA production. *Mol. Genet. Genomics* **276,** 391-401.
Nagai, T., Ibata, K., Park, E. S., Kubota, M., Mikoshiba, K. & Miyawaki, A. (2002) A variant of yellow fluorescent protein with fast and efficient maturation for cell-biological applications. *Nature Biotechnol.* **20,** 87-90 (2002).
Nakagoshi, H., Kanei-Ishii, C., Sawazaki, T., Mizuguchi, G. & Ishii, S. (1992) Transcriptional activation of the c-*myc* gene by the c-*myb* and B-*myb* gene products. *Oncogene* **7,** 1233-1240.
Nakata, Y., Shetzline, S., Sakashita, C., Kalota, A., Rallapalli, R., Rudnick, S. I., Zhang, Y., Emerson, S. G. & Gewirtz, A. M. (2007) c-Myb contributes to G2/M cell cycle transition in human hematopoietic cells by direct regulation of cyclin B1 expression. *Mol. Cell. Biol.* **27,** 2048-2058.
Nakatani, Y. & Ogryzko, V. (2003) Immunoaffinity purification of mammalian protein complexes. *Methods Enzymol.* **370,** 430-444.
Nomura, T., Khan, M.M., Kaul, S.C., Dong, H.D., Wadhwa, R., Colmenares, C., Kohno, I. & Ishii, S. (1999) Ski is a component of the histone deacetylase complex required for transcriptional repression by Mad and thyroid hormone receptor. *Genes Dev.* **13,** 412-423
Nomura, T., Tanikawa, J., Akimaru, H., Kanei-Ishii, C., Ichikawa-Iwata, E., Khan, M. M., Ito, H. & Ishii, S. (2004) Oncogenic activation of c-Myb correlates with a loss of negative regulation by TIF1β and Ski. *J. Biol. Chem.* **279,** 16715-16726
Owen, H. R., Elser, M., Cheung, E., Gersbach, M., Kraus W. L. & Hottiger, M. O. (2007) MYBBP1a is a novel repressor of NF-κB. *J. Mol. Biol.* **366,** 725-736.
Radomski, N. & Jost, E. (1995) Molecular cloning of a murine cDNA encoding a novel protein, p38-2G4, which varies with the cell cycle. *Exp. Cell Res.* **220,** 434-445.
Scheer, U. & Weisenberger D. (1994) The nucleolus. *Curr. Opin. Cell Biol.* **6,** 354-359.
Sherr, C. J. & Weber, J. D. (2000) The ARF/p53 pathway. *Curr. Opin. Genet. Dev.* **10,** 94-99.
Shimizu, K., Kawasaki, Y., Hiraga, S., Tawaramoto, M., Nakashima, N. & Sugino, A. (2002) The fifth essential DNA polymerase phi in Saccharomyces cerevisiae is localized to the nucleolus and plays an important role in synthesis of rRNA. *Proc. Natl. Acad. Sci. USA* **99,** 9133-9138.
Sollner-Webb, B., and Tower, J. (1986) Transcription of cloned eukaryotic ribosomal RNA genes. *Ann. Rev. Biochem.* **55,** 801-830
Takezawa, S., Yokoyama, A., Okada, M., Fujiki, R., Iriyama, A., Yanagi, Y., Ito, H., Takada, I., Kishimoto, M.,

Miyajima, A., Takeyama, K., Umesono, K., Kitagawa, H. & Kato, S. (2007) A cell cycle-dependent co-repressor mediates photoreceptor cell-specific nuclear receptor function. *EMBO J.* **26,** 764-774.

Tavner, F. J., Simpson, R., Tashiro, S., Favier, D., Jenkin,s N. A., Gilbert, D. J., Copeland, N. G., Macmillan, E. M., Lutwyche, .J, Keoug,h R. A., Ishii, S. & Gonda, T. J. (1998) Molecular cloning reveals that the p160 Myb-binding protein is a novel, predominantly nucleolar protein which may play a role in transactivation by Myb. *Mol. Cell. Biol.* **18,** 989-1002.

Taylor, D., Badiani, P. & Weston, K. (1996) A dominant interfering Myb mutant causes apoptosis in T cells. *Genes Dev.* **10,** 2732-2744.

Torrano, V., Navascues, J., Docquier, F., Zhang, R., Burke, L. J., Chernukhin, I., Farrar, D., Leon, J., Berciano, M. T., Renkawitz, R., Klenov,a E., Lafarga, M. & Delgado, M. D. (2006) Targeting of CTCF to the nucleolus inhibits nucleolar transcription through a poly(ADP-ribosyl)ation-dependent mechanism. *J. Cell Sci.* **119,** 1746-1759.

Treiber, D. K., Zhai, X., Jantzen, H. M. & Essigmann, J. M. (1994) Cisplatin-DNA adducts are molecular decoys for the ribosomal RNA transcription factor hUBF (human upstream binding factor). *Proc. Natl. Acad. Sci. U A* **91,** 5672-5676.

Tsai, R. Y. L. & McKay, R. D. G. (2002) A nucleolar mechanism controlling cell proliferation in stem cells and cancer cells. *Genes Dev.* **16,** 2991-3003.

Viatour, P., Merville, M. P., Bours, V. & Chariot, A. (2005) Phosphorylation of NF-κB and IκB proteins: implications in cancer and inflammation. *Trends Biochem. Sci.* **30,** 43-52.

Visintin, R. & Amon, A. (2000) The nucleolus: the magician's hat for cell cycle tricks. *Curr. Opin. Cell Biol.* **12,** 752 (2000).

Weber, J. D., Taylor, L. J., Roussel, M. F., Sherr, C. J. & Bar-Sagi, D. (1999) Nucleolar Arf sequesters Mdm2 and activates p53. *Nature Cell Biol.* **1,** 20-26.

Yang, W., Rogozin, I. B., Koonin, E. V. (2003) Yeast POL5 is an evolutionarily conserved regulator of rDNA transcription unrelated to any known DNA polymerases. *Cell Cycle* **2,** 120–122.

Ying, G. G., Proost, P., van Damme, J., Bruschi, M., Introna, M. & Golay, J. (2000) Nucleolin, a novel partner for the Myb transcription factor family that regulates their activity. *J. Biol. Chem.* **275,** 4152-4158.

Yusufzai, T. M., Tagam,i H., Nakatani, Y. & Felsenfeld, G. (2004) CTCF tethers an insulator to subnuclear sites, suggesting shared insulator mechanisms across species. *Mol. Cell* **13,** 291-298.

Zatsepina, O. V., Voronkova, L. N., Sakharov, V. N. & Chentsov, Y.S. (1989) Ultrastructural changes in nucleoli and fibrillar centers under the effect of local ultraviolet microbeam irradiation of interphase culture cells. *Exp. Cell Res.* **181,** 94-104.

Figure legends

Figure 14. Identification of Mybbp1a complexes. (A) Analysis of the Mybbp1a complexes by glycerol gradient centrifugation. The Mybbp1a complexes were sequentially immunopurified from HeLa cells expressing FLAG/HA-tagged p160^{MBP} using anti-FLAG and anti-HA. The immunopurified complexes were separated on a 10%-40% glycerol gradient by ultracentrifugation, resolved by SDS-PAGE, and visualized by silver staining. The polypeptides identified by mass spectrometric analysis are indicated. (B) Immunoblotting of the Mybbp1a complexes. The glycerol gradient purified Mybbp1a complexes were analyzed by immunoblotting with the antibodies indicated on the right. (C) Co-immunoprecipitation of the Mybbp1a complexes. Lysates of HeLa cells expressing FLAG/HA-p160^{MBP} or no epitope-tagged protein (Mock) were immunoprecipitated with anti-FLAG, and the precipitates were subjected to immunoblot analysis with the antibodies indicated on the right. (D) *In vitro* binding of p160^{MBP} and p67^{MBP}. (Upper) Binding of *in vitro*-translated p160^{MBP} to GST fusion protein containing p67^{MBP}, the N-terminal 326 amino acids fragment (GST-p160N), or the C-terminal 299 amino acids fragment (GST-p160C) of p160^{MBP}. (Lower) The GST fusion proteins used were analyzed by SDS-PAGE followed by coomassie blue staining.

Figure 15. The peptides recovered from p140^{MBP}. Schematic representation of p160^{MBP} is shown at the top. The basic amino acid motifs in the C-terminal region are denoted as solid lines. The peptides recovered from p140^{MBP} are shown in red, while the cluster of basic amino acids in the C-terminal region of p160^{MBP} is indicated in green. The vertical arrows indicate the putative processing sites to generate p67^{MBP} and p140^{MBP}.

Figure 16. Actinomycin D (ActD) induces processing of p160^{MBP} and translocation of the p67^{MBP}/p140^{MBP} complex from the nucleolus to the nucleoplasm. (A) Processing of p160^{MBP} to p67^{MBP} and p140^{MBP} by ActD. HeLa cells expressing FLAG/HA-p160^{MBP} were treated with ActD (50 ng/ml) for 12 h, with cisplatin (40 μM) for 12 h, or UV (30 J/m^2), and the cell lysates were prepared and immunoprecipitated with anti-FLAG antibody. The immunocomplexes were electrophoresed and subjected to Western blotting with a mixture of two polyclonal antibodies raised against the N-terminal 326 residues or C-terminal 298 residues of p160^{MBP}. Western blotting with anti-tubulin (DMIA, Sigma) was performed as the loading control. (B) ActD induces a translocation of FLAG/HA-Mybbp1a and nucleophosmin from the nucleolus to the nucleoplasm. HeLa cells expressing

FLAG/HA-p160^{MBP} were treated with ActD (50 ng/ml) for 12 h, fixed, and subjected to indirect immunofluoresecent staining with anti-FLAG (Cy3, red) and anti-nucleophosmin (Cy3, red), and visualized using confocal microscopy. DNA was visualized by staining with TOTO-3 iodide (blue).

Figure 17. Time-lapse video analysis of translocation of Mybbp1a from the nucleolus to the nucleoplasm. (A) A retrovirus vector encoding Venus-p160^{MBP} was generated, and HeLa cells were transduced with a recombinant retrovirus. Cell lysates from the tranductants and the mock transduced cells were used for Western blotting with anti-GFP antibody. (B) Selected video frames from a time-lapse recording of HeLa cells expressing Venus-p160 ^{MBP}, showing five representative pictures derived from a 3 h time course after addition of ActD (50 ng/ml). A typical pattern, from the single cell surrounded by a square, is shown below with higher magnification. (C) Translocation of Mybbp1a is not reversible when ActD was washed out. HeLa cells expressing Venus-p160 ^{MBP} were treated with ActD (50 ng/ml) for 12 h, and then ActD was washed out. Selected video frames from a time-lapse recording of cells after ActD removal are shown.

Figure 18. ActD induces a translocation of nucleophosmin and nucleolin, but not nucleostemin and EBP1, from the nucleolus to the nucleoplasm. HeLa cells were treated with ActD (50 ng/ml) for 24 h, fixed, and subjected to indirect immunofluoresecent staining with anti-nucleostemin (Alexa Fluor 488, green) and anti-nucleophosmin (Cy3, red) (A), or anti-EBP1 (Alexa Fluor 488, green) and anti-nucleolin (Cy3, red) (B), and visualized using confocal microscopy. DNA was visualized by staining with TOTO-3 iodide (blue). A typical pattern, from the single cell surrounded by a square, is shown below with higher magnification, indicating the localization of EBP1 at the nucleoli in the ActD-treated cells. Arrowheads show the nucleoli.

Figure 19. Ribosomal stress induces translocation of Mybbp1a and nucleophosmin from the nucleolus to the nucleoplasm. NIH3T3 cells were treated with ActD (50 ng/ml), cisplatin (40 μM) or UV (30 J/m^2). Twelve hours after treatment, cells were fixed, and subjected to indirect immunofluoresecent staining as described in the legend to Figure 3B with anti-Mybbp1a (Alexa Fluor 488, green) and anti-nucleophosmin (Cy3, red), and visualized using confocal microscopy. Anti-Mybbp1a antibody used here was raised against the N-terminal 326 residues of p160^{MBP}, and recognize p160^{MBP}, p140^{MBP}, and p67^{MBP}. DNA was visualized by staining with TOTO-3 iodide (blue).

Figure 21. (A) Co-immunoprecipitation of Mybbp1a with CTCF and PARP. Lysates of HeLa cells expressing FLAG/HA-p160^{MBP} or no epitope-tagged protein (Mock) were immunoprecipitated with anti-FLAG, and the precipitates were subjected to immunoblot analysis with the antibodies indicated on the left. (B) Detection of CTCF in the purified Mybbp1a complexes. The glycerol gradient purified Mybbp1a complexes, which was shown in Figure 1B, were analyzed by immunoblotting with the anti-CTCF antibody. (C) HeLa cells were treated with ActD (50 ng/ml) for 24 h, fixed, and subjected to indirect immunofluoresecent staining with anti-CTCF or anti-PARP (Alexa Fluor 488, green) and anti-histone H1 or anti-nucleophosmin (Cy3, red), and visualized using confocal microscopy. DNA was visualized by staining with TOTO-3 iodide (blue).

Figure 21. Proposed model for the translocation of Mybbp1a complex from the nucleolus to the nucleoplasm. The large Mybbp1a complex containing p160^{MBP}, nucleostemin, nucleophosmin, nucleolin and various ribosomal subunit proteins is localized in the nucleolus. On the other hand, the small complex containing p67^{MBP}, p140^{MBP}, EBP1, nucleophosmin, and nucleolin is localized in the nucleoplasm. Although the Mybbp1a molecules can form a dimer or an oligomer, it is unknown at present whether the large and small complexes contain the p160^{MBP} homodimer or homoolimer and the p140^{MBP}/p67^{MBP} heterodimer or heterooligomer, respectively. Inhibition of ribosomal biogenesis induces processing of p160^{MBP} into p140^{MBP} and p67^{MBP} and a translocation of the small complex from the nucleolus to the nucleoplasm. Presence of various ribosomal subunit proteins in the nucleolar large complex suggests that it acts to stimulate the ribosome biogenesis. On the other hand, since p67^{MBP} suppresses c-Myb-dependent transcription, the nucleoplasmic small complex may inhibit the c-Myb-dependent cell cycle progression and apoptosis block.

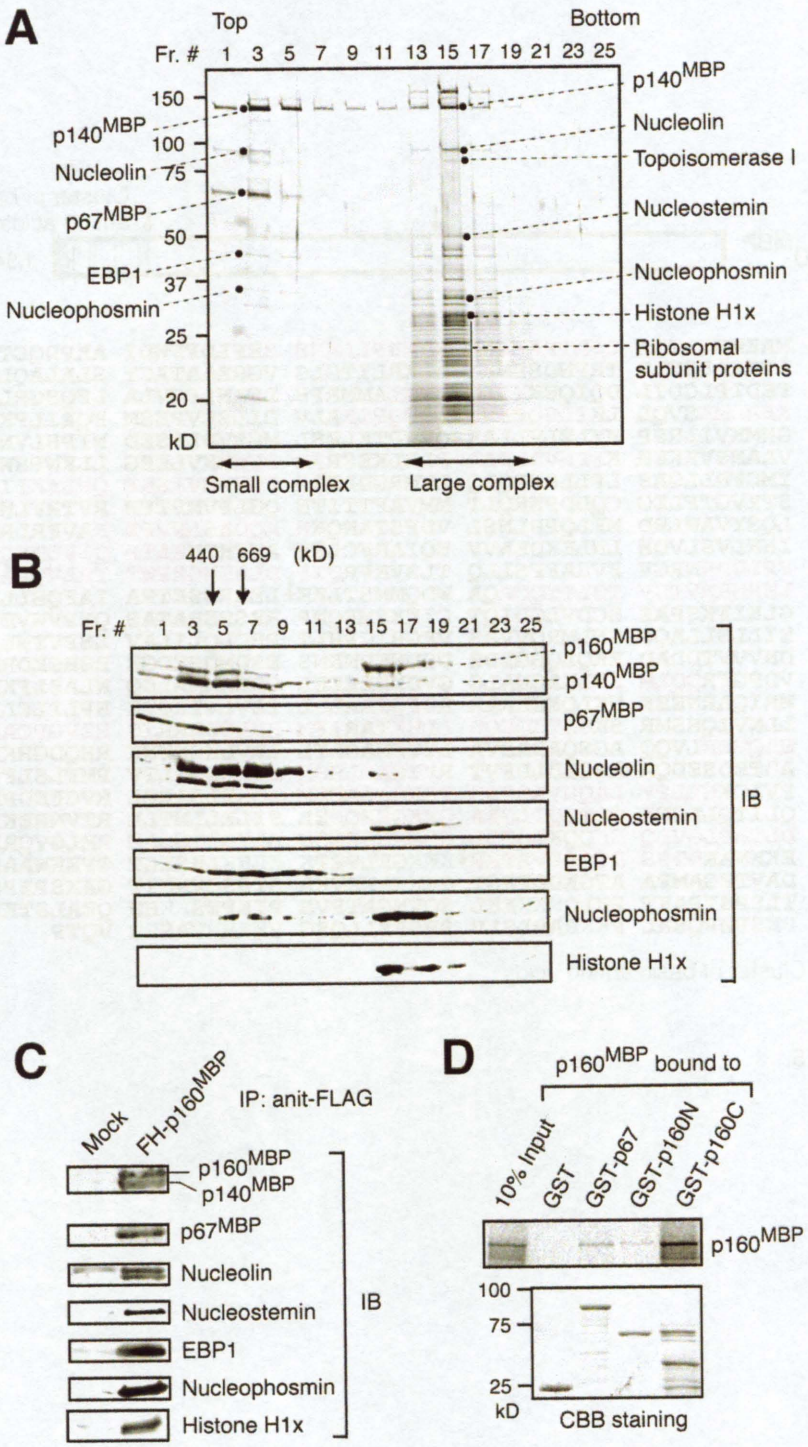
A
Top
Bottom
Fr. # 1 3 5 7 9 11 13 15 17 19 21 23 25
150
100
75
50
37
25
20
kD
p140MBP
Nucleolin
p67MBP
EBP1
Nucleophosmin
p140MBP
Nucleolin
Topoisomerase I
Nucleostemin
Nucleophosmin
Histone H1x
Ribosomal subunit proteins
Small complex
Large complex
B
440 669 (kD)
Fr. # 1 3 5 7 9 11 13 15 17 19 21 23 25
p160MBP
p140MBP
p67MBP
Nucleolin
Nucleostemin
EBP1
Nucleophosmin
Histone H1x
IB
C
Mock
FH-p160MBP
IP: anit-FLAG
p160MBP
p140MBP
p67MBP
Nucleolin
Nucleostemin
EBP1
Nucleophosmin
Histone H1x
IB
D
p160MBP bound to
10% Input
GST
GST-p67
GST-p160N
GST-p160C
p160MBP
100
75
25
kD
CBB staining

Fig. 14.

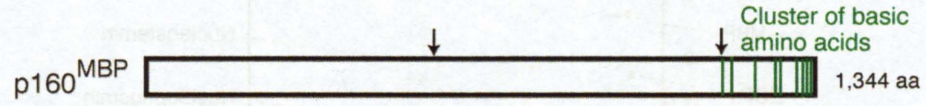


```
   1 MAEMKSPTKA EPATPAEAAQ SDRHSLLEHS REFLDFFWDI AKPDQETRLR
  51 ATEKLLEYLR TRPNDSEMKY ALKRLITGLG VGREAATACY SLALAQLLQS
 101 FEDIPLCDIL DQIQEKYSLQ AMNKAMMRPS LFANLFGVLA LFQSGRLVKD
 151 KEALMKSVQL LKILSQHPNH LQGQPIKALV DILSEVPESM FQEILPKVLK
 201 GNMKVILRSP KYLELFLLAK QRVPTKLESL MGSVDLFSED NIPSLVNILK
 251 VAANSVKKEH KLPNVALDLL RLALKESRFE LFWKKVLEEG LLKNPSWTSS
 301 YMCFRLLGAS LPLLSEEQLQ LVMRGDLIRH FGENMVISKP QNLFKIIPEI
 351 STYVGTFLEG CQDDPKRQLT MMVAFTTITN QGLPVMPTFW RVTRFLNAEA
 401 LQSYVAWLRD MFLQPDLNSL VDFSTANQKR AQDASLNVPE RAVFRLRKWI
 451 IHRLVSLVDH LHLEKDEAVV EQIARFCLFH AFFKTKKATP QIPETKQHFS
 501 FPLDDRNRGV FVSAFFSLLQ TLSVKFRQTP DLAENGKPWT YRLVQLADML
 551 LNHNRNVTSV TSLTTQQRQA WDQMMSTLKE↓LEARSSETRA IAFQHLLLLV
 601 GLHIFKSPAE SCDVLGDIQT CIKKSMEQNP RRSRSRAKAS QEPVWVEVMV
 651 EILLSLLAQP SNLMRQVVRS VFGHICPHLT PRCLQLILAV LSPVTNEDED
 701 DNVVVTDDAD EKQLQHGEDE DSDNEDNKNS ESDMDSEDGE ESEEEDRDKD
 751 VDPGFRQQLM EVLKAGNALG GVDNEEEEEL GDEAMMALDQ NLASLFKEQK
 801 MRIQARNEEK NKLQKEKKLR RDFQIRALDL IEVLVTKQPE HPLILELLEP
 851 LLNVIQHSMR SKGSTKQEQD LLHKTARIFM HHLCRARRYC HEVGPCAEAL
 901 HAQVERLVQQ AGSQADASVA LYYFNASLYL LRVLKGNTNK RHQDGHKLHG
 951 ADTEDSEDQA ANCLDLDFVT RVYSASLESL LTKRNSSLTV PMFLSLFSRY
1001 PVICKNLLPV LAQHVAGPSR PRHQAQACLM LQKTLSAREL RVCFEDPEWE
1051 QLITQLLGKA TQTLQTLGEA QSKGEHQKEL SILELLNTLL RTVNHEKLSV
1101 DLTAPLGVLQ SKQQKLQQSL↓QQGNHSSGSN RLYDLYWQAM RMLGVQRPKS
1151 EKKNAKDIPS DTQSPVSTKR↓KKKGFLPETK KRKKLKSEGT TPEKNAASQQ
1201 DAVTEGAMPA ATGKDQPPST GKKKRKRVKA STPSQVNGIT GAKSPAPSNP
1251 TLSPSTPAKT PKLQKKKEKL SQVNGATPVS PIEPESKKHH QEALSTKEVI
1301 RKSPHPQSAL PKKRARLSLV SRSPSLLQSG VKKRRVASRR VQTP
```

Cluster of basic amino acids

Fig. 15.

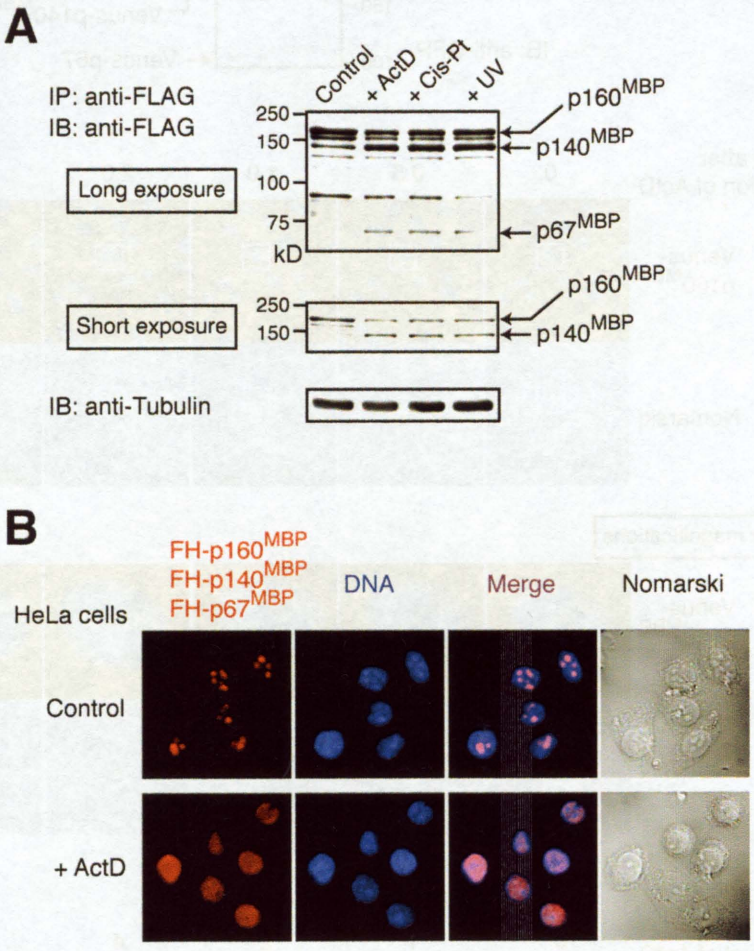
A
IP: anti-FLAG
IB: anti-FLAG
Control
+ ActD
+ Cis-Pt
+ UV
250
150
100
75
kD
p160MBP
p140MBP
p67MBP
Long exposure
Short exposure
IB: anti-Tubulin
B
FH-p160MBP
FH-p140MBP
FH-p67MBP
DNA
Merge
Nomarski
HeLa cells
Control
+ ActD

Fig. 16.

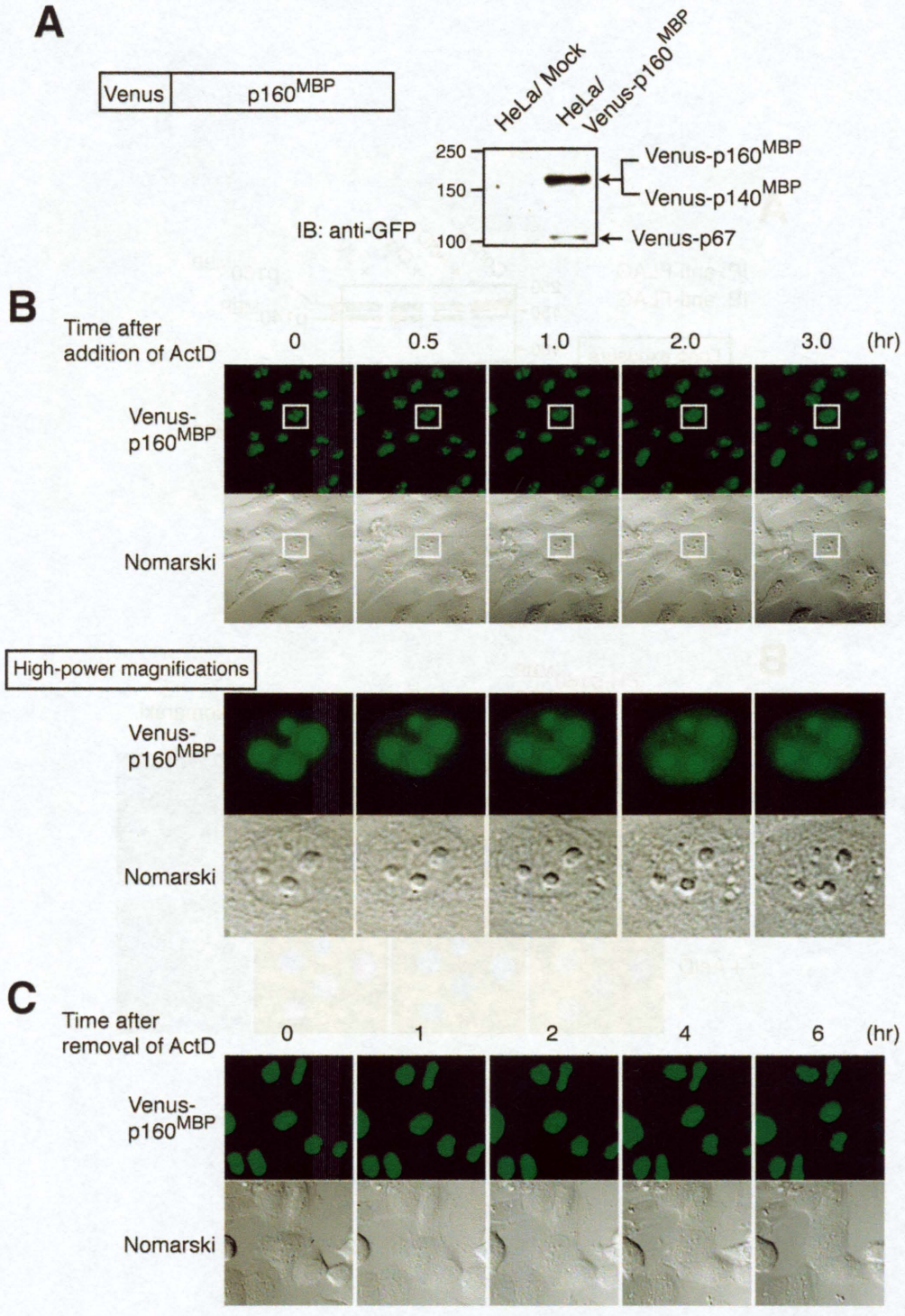
A
Venus
p160MBP
HeLa/ Mock
HeLa/ Venus-p160 MBP
250
150
100
IB: anti-GFP
Venus-p160MBP
Venus-p140MBP
Venus-p67
B
Time after addition of ActD
0
0.5
1.0
2.0
3.0
(hr)
Venus-p160MBP
Nomarski
High-power magnifications
Venus-p160MBP
Nomarski
C
Time after removal of ActD
0
1
2
4
6
(hr)
Venus-p160MBP
Nomarski

Fig. 17.

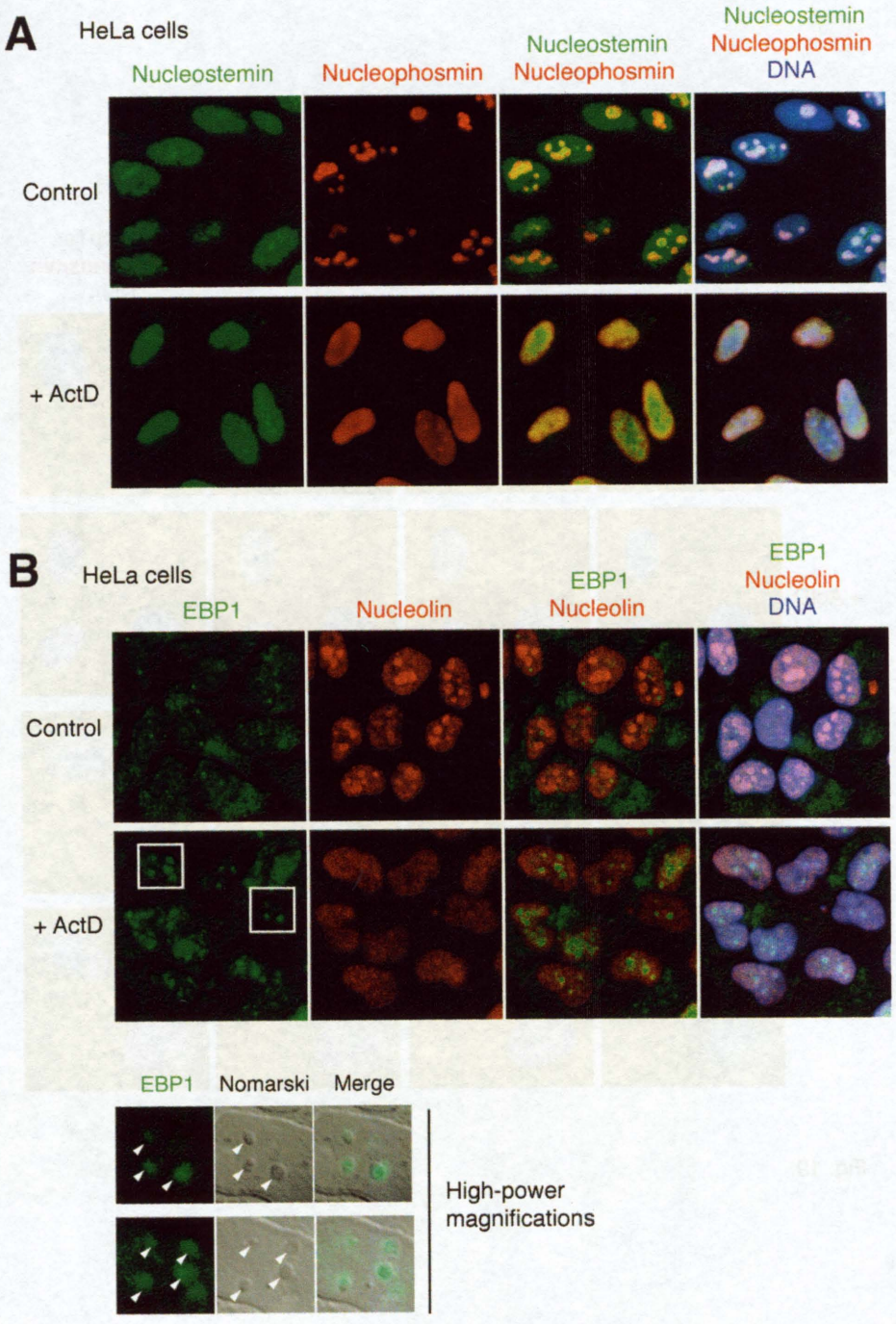
A
HeLa cells
Nucleostemin
Nucleophosmin
Nucleostemin
Nucleophosmin
Nucleostemin
Nucleophosmin
DNA
Control
+ ActD
B
HeLa cells
EBP1
Nucleolin
EBP1
Nucleolin
EBP1
Nucleolin
DNA
Control
+ ActD
EBP1
Nomarski
Merge
High-power
magnifications

Fig. 18.

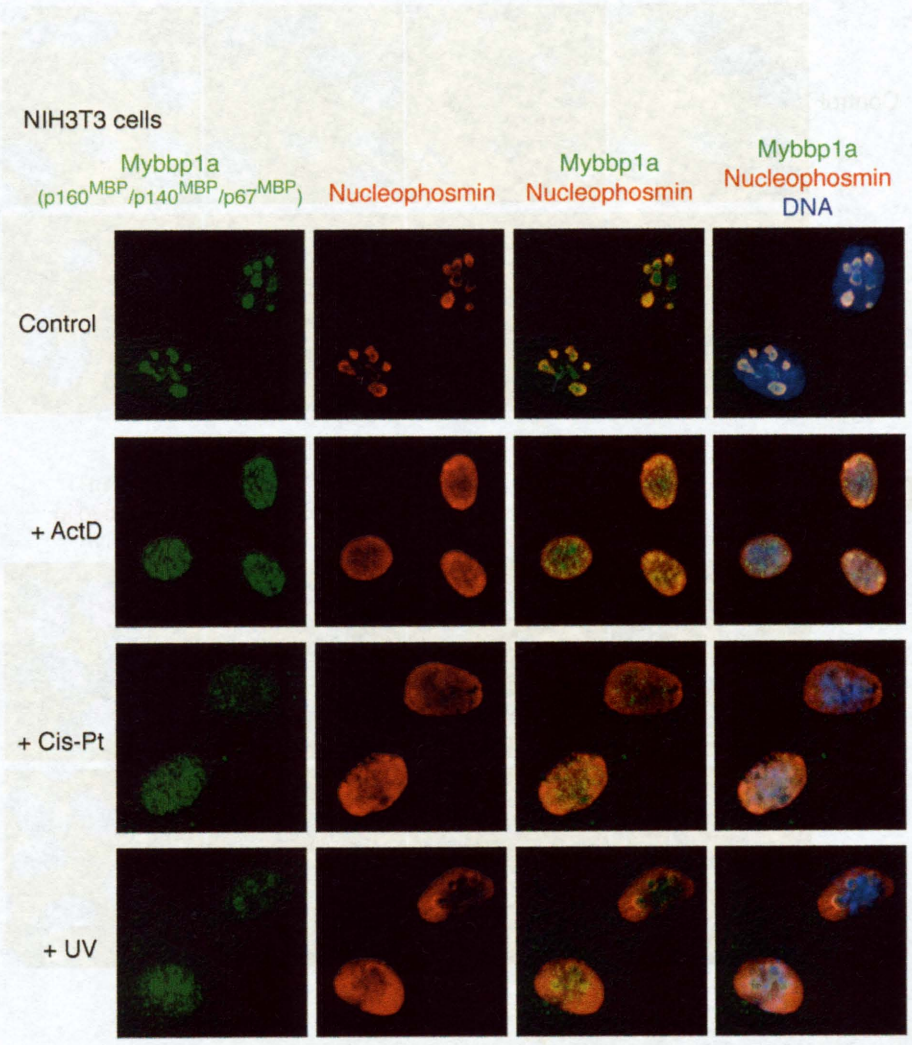
NIH3T3 cells
Mybbp1a
(p160MBP/p140MBP/p67MBP)
Nucleophosmin
Mybbp1a
Nucleophosmin
Mybbp1a
Nucleophosmin
DNA
Control
+ ActD
+ Cis-Pt
+ UV

Fig. 19.

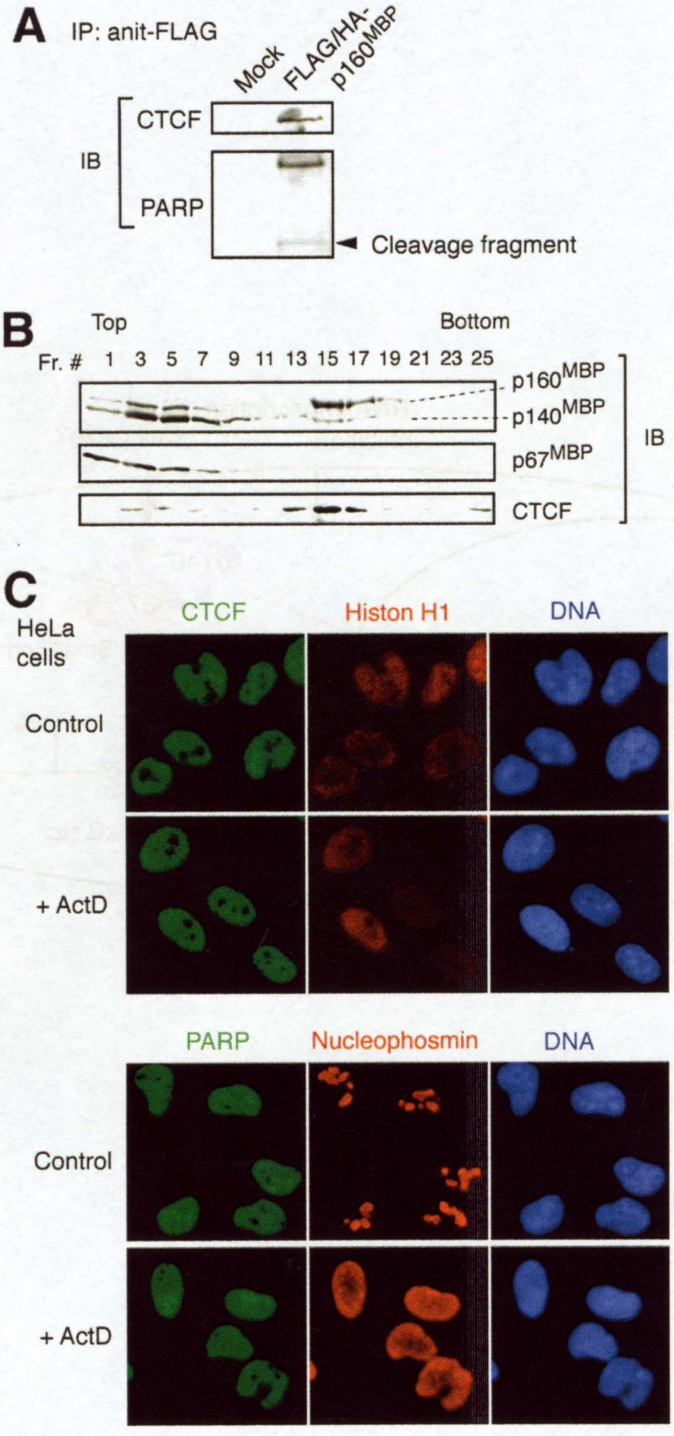
A
IP: anit-FLAG
Mock
FLAG/HA-p160MBP
CTCF
IB
PARP
Cleavage fragment
B
Top
Bottom
Fr. # 1 3 5 7 9 11 13 15 17 19 21 23 25
p160MBP
p140MBP
p67MBP
CTCF
IB
C
HeLa cells
CTCF
Histon H1
DNA
Control
+ ActD
PARP
Nucleophosmin
DNA
Control
+ ActD

Fig. 20.

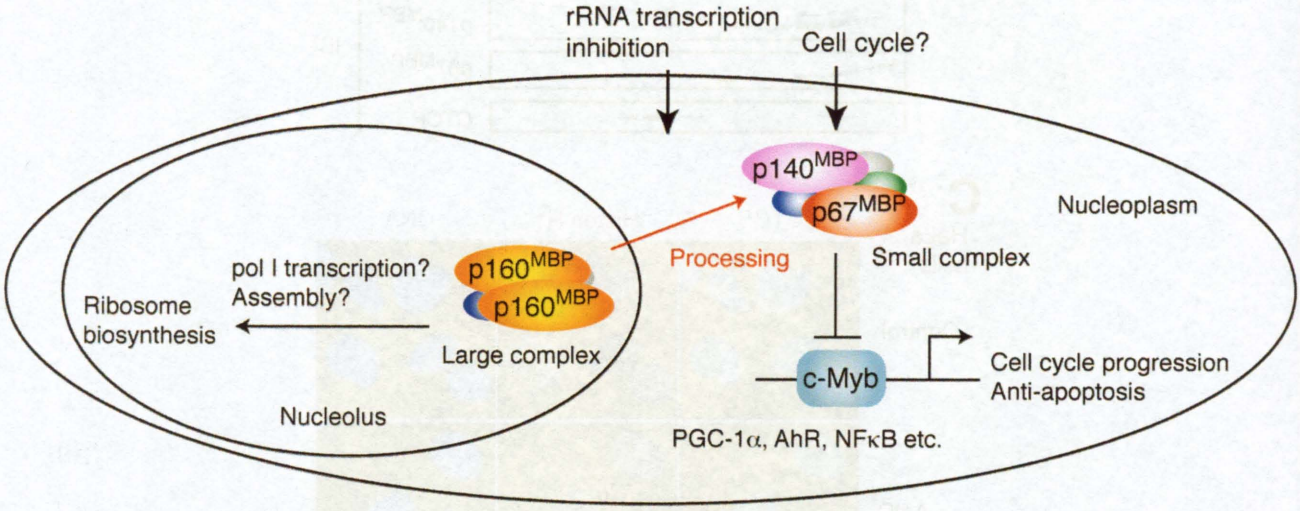
rRNA transcription inhibition
Cell cycle?
p140MBP
p67MBP
Nucleoplasm
Processing
Small complex
pol I transcription?
Assembly?
Ribosome biosynthesis
p160MBP
p160MBP
Large complex
c-Myb
Cell cycle progression
Anti-apoptosis
Nucleolus
PGC-1α, AhR, NFκB etc.

Fig. 21.

総括

本研究において、私は、dREAM/Myb-MuvB-like 複合体とは異なる新たな B-Myb 複合体を精製し、この複合体が、B-Myb, Clathrin, Filamin を含むことから、Myb-Clafi 複合体と名付けた。Myb-Clafi 複合体は、細胞周期の中でも間期には存在せず分裂期にのみ存在し、かつ dREAM/Myb-MuvB-like 複合体に比べて存在量が少ないために、これまで精製されなかったと考えられる。さらに Myb-Clafi 複合体は比較的安定なため、420 mM の塩濃度存在下で、精製することができた。この塩濃度下では、比較的不安定な dREAM/Myb-MuvB-like 複合体は解離してしまうため、Myb-Clafi 複合体のみが精製できたと考えられる。ちなみに、dREAM/Myb-MuvB 複合体は 100 mM の塩濃度存在下で、精製されることが報告されている。

さらに B-Myb の C 端側の一部を欠損する M14 変異体は、Myb-Clafi 複合体を形成することができないが、dREAM/Myb-MuvB-like 複合体を形成することができ、一群の G2/M 移行に必要な遺伝子の転写を誘導できることを示した。そして、この M14 変異体を endogenous B-Myb の代わりに発現させると、有糸分裂紡錘体の形成が不全となることを明らかにした。一昨年、Clathrin が、分裂紡錘体の形成に必要であることが Nature 誌に報告されたが、本研究は、Clathrin が B-Myb や Filamin と共に、分裂紡錘体の形成に関与することを示したものである。Clathrin は Tubulin と結合して、それを束化することによって、分裂紡錘体の強化に関与しているのではないかと推定されている。B-Myb と Filamin の作用メカニズムについては、今後の研究の進展を待たなければならないが、B-Myb は多くの因子と相互作用するタンパク質表面を有していることから、Clathrin と Filamin に結合することによって、アダプターとして機能している可能性がある。また、Filamin はアクチンと結合することが知られている。アクチンはアクチンリングの形成を介して細胞分裂を制御することから、紡錘体とも何らかの相互作用があるのではないかと推定されているが、これまでに直接的的な知見は得られていない。Myb-Clafi 複合体中の Filamin がアクチンと紡錘体との相互作用を仲介する可能性は、大変魅力的であり。今後の研究の発展に期待したい。

これまで、*dmyb* や B-*myb* 変異体におけるゲノム不安定性が、dREAM/Myb-MuvB-like 複合体による G2/M 期移行の異常だけによって、完全に説明できるか否かについては不明であった。本研究によって、B-Myb は dREAM/Myb-MuvB-like 複合体を形成して、G2/M 期移行に必要な遺伝子の転写を誘導するだけでなく、Myb-Clafi 複合体を形成して、有糸分裂紡錘体の機能を制御することが示された。この 2 つの複合体は、M 期への移行と、それに続く細胞分裂を、協調的に進行させるために、協力して機能していると考えられる、特筆すべきは、後者の機能だけが欠損しても、ゲノム不安定性が見られることである。ゲノム不安

定性は、多くのタイプのがんを発症することが知られているので、B-Myb は Myb-Clafi 複合体を形成して、がん抑制因子として機能するとも言える。以上のように、B-Myb を含む新たな複合体の精製と解析によって、分裂紡錘体の機能制御という B-Myb の新たな機能が明らかとなった。

一方、Mybbp1a 複合体の精製と解析によって、Mybbp1a が、核小体に局在する大きな複合体と、核質に局在する小さな複合体に分けられること、前者には $p160^{MBP}$ が、一方後者には $p140^{MBP}$ と $p67^{MBP}$ が含まれることが示された。$p140^{MBP}$ は、$p160^{MBP}$ の C 末端の核小体局在シグナルを欠いたものであり、リボソームの生合成を停止させる一群のストレス（ActD、cisplatin、UV）によって、$p160^{MBP}$ が $p140^{MBP}$ と $p67^{MBP}$ にプロセシングされ、核小体から核質へ移行することが明らかにされた。核小体に局在する大きな Mybbp1a 複合体は、その構成因子から判断して、rRNA 転写やリボソーム形成を促進し、リボソームの生合成を正に制御していると考えられる。一方、核質に移行する小さな Mybbp1a 複合体は、c-Myb に結合して c-Myb 依存的な転写活性化を阻害すると考えられる。リボソームの生合成は、細胞機能の中でも特に大きなエネルギーを必要とし、細胞増殖はリボソームの生合成と密接にリンクしている。したがって、リボソーム生合成が低下した時に、Myb などの転写因子の活性を抑制し、細胞周期を停止させることは、大変理にかなった現象である。以上のように、Myb に結合する因子 Mybbp1a の複合体の解析によって、「Myb 活性とリボソーム生合成のリンク」という新たな Myb の制御機構が明らかにされた。